2–1–3 Data Processing

The assay results of the above four components of the 1,031 samples were input into computor, together with the data of geological units in the vicinities of the sampling stations. They were statistically processed and placed under various kinds of analysis. Table A–5 shows the assay results.

(1) Single Component Analysis

Histograms and cumulative frequency distribution diagrams were produced for the purpose of extracting anomalous values of each component (Fig. II–12 and 13).

The histogram for As does not show correct logarithmic normal distribution since 86.4 per cent of the values are below the detection limit. On the other hand, the histograms for Pb and Zn show correct logarithmic normal distribution, and Cu is almost the same as the formers.

In cumulative frequency distribution diagrams, each component shows a linear distribution, and no distinct turning point is not observed.

From the above $x + 2\sigma$ the anomalous threshold value of, which occupies about 2.5 per cent of the whole part was adopted (t). This value has also been generally used in geochemical surveys. Meanwhile, the value occupying about five per cent of the whole was adopted as a supplementary threshold value (t'). Thus, it was defined that the values higher than (t') and lower than (t) are the lower threshold values and those more than (t) the higher threshold values.

Cumulative frequency distribution diagrams (Lipeltier, 1964) was used for the sake of convenience to determine (t) and (t') of each component, the results of which are shown in Table II–3. Anomalous values almost similar to those of CPRM (1982) were obtained. CPRM determined that the values higher than 98 per cent as the anomalous value of the first order and those between 95 to 98 per cent as those of the second order.

The correlation of each component is as shown in Table II–4. Although a strong correlation is observed in Cu, Pb and Zn, As is very low in correlation with any other components.

(2) Multivariate Analysis

Also various methods are used for multivariate analysis, factor analysis is effective as the method of analysis to obtain scientific simplicity by explaining the fluctuation caused by multivariate by a small number of representative and hypothetical fluctuation factors. The factor analysis is the method to explain the relation between a given sample and its mineralization or the characteristics of country rocks by indicating the factor score of each factor in order to grasp what each sample holds what kind of factor to what extent.

As the result of analysis by processing data by the varimax method, one of the methods of factor analysis, using computor, the following three factors (Table II–5) were extracted: the first

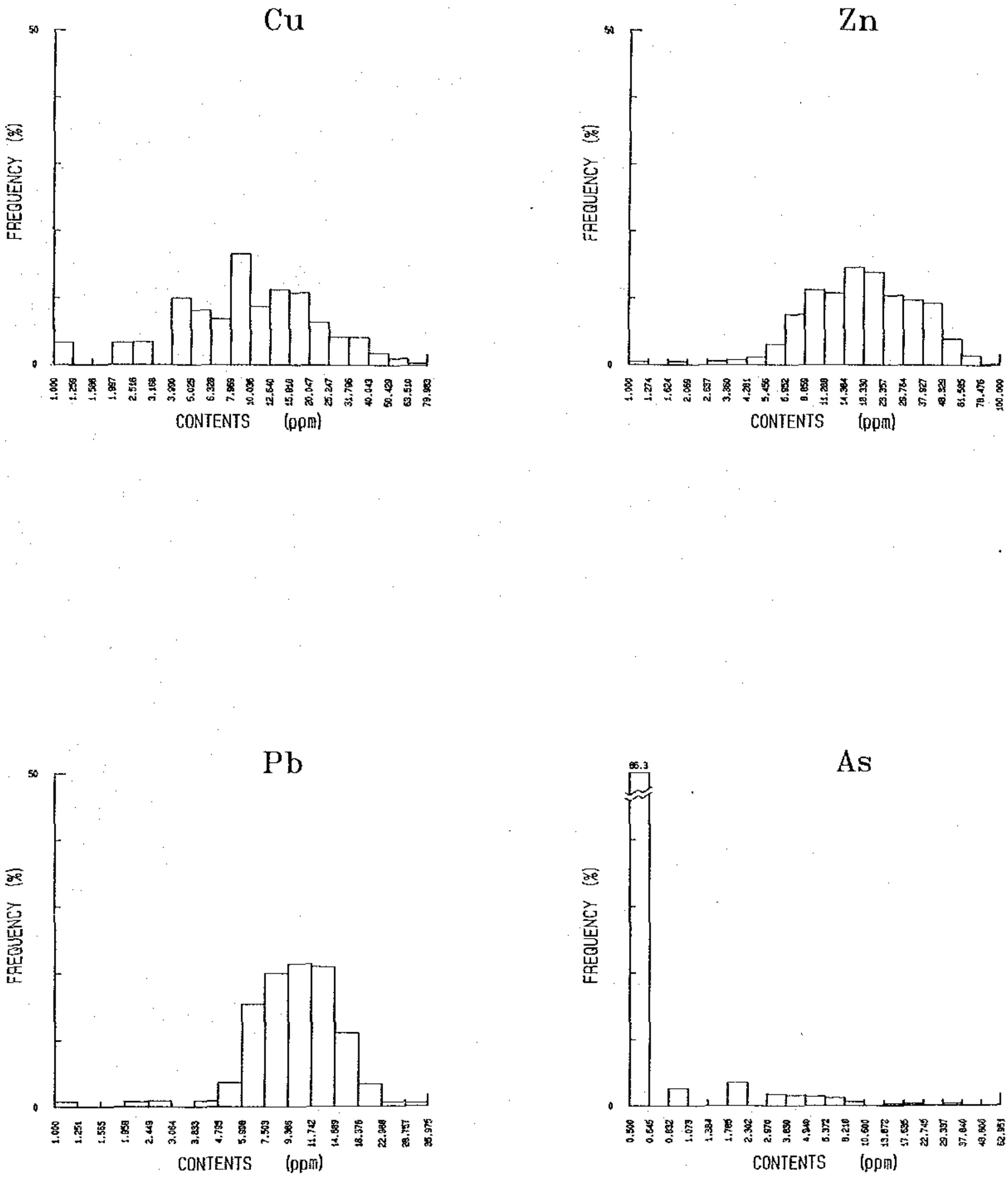

Fig. II—12 Histogram for Cu, Pb, Zn and As of Stream Sediment

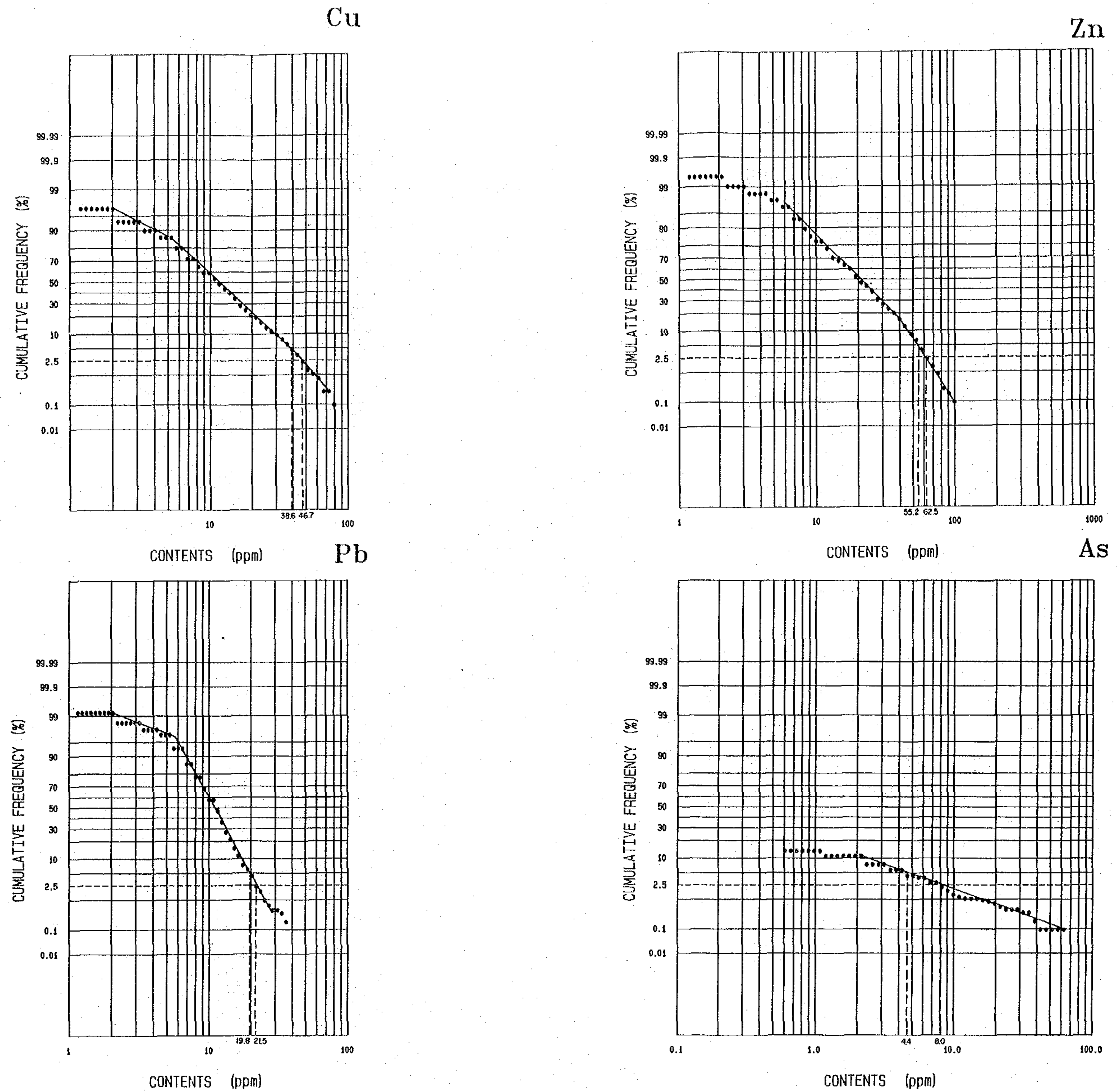

Fig. II–13 Cumulative Frequency Distribution of Cu, Pb, Zn and As of Stream Sediment

Table II–3 Results of Simplified Statistical Treatment of Geochemical Data of Stream Sediments

Element	Max. (ppm)	Min. (ppm)	Mean (ppm)	t' (5%) (ppm)	t (2.5%) (ppm)
Cu	80	5 (1)	9.748	38.6	46.7
Pb	36	5 (1)	9.783	19.8	21.5
Zn	100	5 (1)	17.776	55.2	62.5
As	63	1 (0.5)	(0.646)	(4.4)	(8.0)

Table II–4 Correlation Matrix of Four Elements of Geochemical Data of Stream Sediments

	Cu	Pb	Zn	As
Cu	1.000			
Pb	0.576	1.000		
Zn	0.741	0.604	1.000	
As	0.261	0.264	0.234	1.000

Table II–5 Results of Factor Analysis of Geochemical Data of Stream Sedimenta

Factor Loadings (varimax rotation)				Communality
Element \ Factor No.	Factor 1	Factor 2	Factor 3	
Cu	0.705	0.394	0.304	0.7440
Pb	0.345	0.417	0.558	0.6044
Zn	0.684	0.336	0.406	0.7452
As	0.062	0.507	0.056	0.2642
Factor contributions	88.938%	7.815%	3.580%	

factor being Cu-Zn, the second Pb-As and the third Pb-Zn.

2–1–4 Results of Interpretation

(1) Single Component Analysis

The anomalous values of each component obtained in the data processing stage were plotted on the drainage map at 1:50,000 (PL. II–10 to 13).

As mentioned above, the sampling stations are small in number in the semi-detailed survey area in the northern part, because the sampling was carried out only for the main rivers by making reference to the results of the survey by CPRM (1982). The drainage systems in which anomalous values were detected in the current survey, however, are almost consistent with those reported by CPRM (1982).

1. Copper (Cu)

The most sizable geochemical anomalous zone is found in the Pip_1 and Pip_3 formations in the vicinity of the camp site of Billington Metais Ltda. in slightly northeast of the central part of the area. In addition, anomalies on a small scale are distributed at several places including some parts of Alvo 9P, 1P and 6P, as well as in the southwest of 11P in the semi-detailed survey area. They are also partially distributed in the Pip_5 formation in the middle reaches of Rio Mocambão in the northwest of the central part of the area, in the Pip_3 formation and the Pip_4vs member in the central part of the area, as well as in the Pip_3 formation in the southern part of the area.

Among these anomalies, those related to Alvo and those scattered in the Pip_4vs member in the central part were detected in the drainage system flowing through the boundary between amphibolite and schist which corresponds to the ore horizon. This evokes interest in the relationship with copper mineralization. It is interpreted that the anomalies in the Pip_1 and Pip_3 formations were caused by leaching of copper component contained in the country rock itself, since the background area is underlain by amphibolite derived from the basic rocks.

2. Lead (Pb)

The areas which can be extracted as the geochemical anomalous zones are distributed in Alvo 2P and Alvo 7P, Alvo 1P and Pm_1xt formation in the western part of the area. The anomaly at Alvo 2P is that of the high anomalous zone caused by the C-1 deposit, and it is considered possible that the anomalies at Alvo 7P and Alvo 1P are caused by mineralization similar to that of the C-1 deposit. The anomalous zone in the western part is assumed to be in close relation with that of As, which have been affected by hydrothermal solution ascended along the fault zone. In addition, small anomalies are partially scattered in some parts of Alvo 10P and 9P, in the Pip_3 formation in the northeast of the central part, and in the formations such as Pip_5, Pmsm and Pm_1 xt from the northwestern part to the southwestern part of the area. It is interesting that the anomalies at Alvo 10P and 9P are the ones caused by lead mineralization.

The anomaly in the Pip_3 formation in the central part is considered to have been present in the basic rocks primarily, and those scattered from the northwestern part to the southwestern part are interpreted to be related to hydrothermal water ascended along the fault. However, particular attentions should be paid with regard to the anomaly detected at slight northeast of the central part, since the schistose terrain of the Pip_4 vs is included in a part of the river basin as the background.

3. **Zinc (Zn)**

As the anomalous zones of zinc, a part of Alvo 12P, the Pip_1 and Pip_3 formations at slightly northeast of the central part and the area in the western part, which is overlapped with Pb and As anomalous zones, were extracted. The anomaly at Alvo 12P is found in the schistose rocks, and this area was also extracted as anomalous zone in the soil geochemical survey described later, indicating the possibility of the occurrence of zinc mineralization. The anomalous zone in the western part of the area is thought to be related to hydrothermal water ascended along the fault zone.

In addition, the anomalies presumably caused by zinc mineralization are also scattered in the southwest of Alvo 2P, Alvo 11P, and in the Pip_4 vs formation in the central part. Although anomalies scattered in the Pip_3 and Pip_5 formations have been detected, no showing of ore deposits has been reported.

4. **Arsenic (As)**

A sizable anomalous zone and small anomalies of arsenic are scattered in the Pm_1 xt member in the western part of the area and in the vicinity.

The Pm_1 xt member in which these anomalies are distributed consists of fine-grained schist derived from pelitic sedimentary rocks, and it cannot be interpreted that As is contained in the country rock itself because the possibility of occurrence of arsenic deposit of sedimentary origin in this horizon has not been reported. On the other hand, since these anomalies are distributed along the fault zone of N-S system, it can be interpreted that these anomalies are associated with the hydrothermal solution ascended along the fault of N-S system.

(2) Multivariate Analysis

PL. II–14 to 16 show the analytical diagrams of the first factor, the second factor and the third factor.

1. **First Factor (Cu-Zn)**

Based on the definitions that those with factor contributions of not less than 1 (one) are the high factor contribution, and those between 0.5 and 1 (one) the moderate factor contribution, the zones of moderate to high factor contribution were extracted at Alvo 2P, 1P, 6P, 9P and 11P to 12P in the semi-detailed survey area. They are almost consistent with the Cu and Zn anomalous zones extracted by single component analysis. Most of these anomalous zones are found in the Pip_1 and Pip_3 formations, in which the geology of the same horizon as that of the known ore deposit or the country rock is contained.

On the other hand, zones of moderate to high factor contributions were extracted in the central to the southern parts of the area. In particular, the Pip_4vs member which can be correlated to the same horizon as the country rock immediately above the ore deposit is widely distributed. In the zone in the central part of the area. The single component analysis indicates that Cu, Pb and Zn anomalies are also scattered in this formation. Other zones include those concentrated in the Pip_1 and Pip_3 formations in the northeast of the central part of the area (in the vicinity of the Billington Metais camp), those concentrated in the Pip_5 formation in slightly northwest of the central part and those scattered in the Pip_3 formation in the southern part.

As in the above, the first factor is considered to have reflected the characteristic of the country rocks represented by amphibolites such as Pip_1 and Pip_3 derived from basic rock, and it is thought that something to characterize Cu-Zn mineralization would be contained in the terrain underlain by schistose rocks.

2. Second Factor (As-Pb)

As the result of factor contribution ranking, as seen in case of the first factor, moderate factor contributions were extracted at Alvo 2P, 9P, 1P and 6P.

Although zones of high factor contribution were extracted in the Pm_1xt and Pmsm formations in the western part of the area, as well as in the Pip_3 and Pip_5 formations in the southern part, no lead mineralized zone was found in both places. These areas as close to the fault, and are well consistent with the As anomaly.

On the other hand, no zone of moderate to high factor contribution was extracted in the vicinity of the Pip_4vs formation in the central part of the area, but high factor contribution on a small scale is sparcely scattered in this area.

Thus it is thought that the second factor mainly reflects some hydrothermal alteration ascended along the fault. Although it might be the case that something to characterize the lead mineralization would be contained in the surrounding area of the C-1 deposit, the question whether it is primary or not would have to be left for future investigation.

3. Third Factor (pb-Zn)

As the result of the analysis conducted in the same procedures as in the first and the second factors, moderate to high factor contributions were extracted in all the Alvo areas except for Alvo 11P in the semi-detailed survey area. These areas included all the lead and zinc anomalies detected in the single component analysis.

In addition, zones of moderate to high factor contribution were extracted in the zone centering on the Pip_4vs formation in the central part of the area, in the zone centering on the Pip_5 formation in slightly northwest of the central part and in the Pip_3 and Pip_5 formations in the southern part.

This factor is thought to have mainly reflected the lead and zinc mineralization.

2–1–5 Relation between Geochemical Anomaly and Mineralization

While many geochemically anomalous zones were extracted by single component analysis and multivariate analysis, the investigation of relationship between these anomalous zones and mineralization resulted in extracting the following six important geochemically anomalous areas (PL. II–17, Fig. II–14).

① Semidetailed survey area (Cu-Pb-Zn)

② Surrounding area of the Pip_4vs member in the central part of the regional survey area (Cu-Zn-Pb)

③ In the Pip_1 and Pip_3 formations in the northeast of the central part of the regional survey area (Cu-Zn)

④ In the Pip_5 formation in the northwest of the central part of the regional survey area (Cu-Pb-Zn)

⑤ In the Pm_1xt and Pmsm formation in the western part of the regional survey area (As-Pb)

⑥ In the Pip_3 and Pip_5 formations in the southern part of the regional survey area (As-Pb(-Zn-Cu))

For the above six areas, the following remarks are to be noted:

① Semi-detailed survey by the soil geochemical method was conducted this year in the survey area, and the detailed survey stage has started.

② When taking into consideration the distribution of the geology correlated to the same horizon corresponding to the country rock of ore deposit in the semi-detailed survey area, Cu-Pb-Zn mineralization is also expected in this area. Thus the area seems to be the most important target for future surveys.

③ It is thought that Cu-Zn component contained in the basic rock in the area has been leached and concentrated in some part.

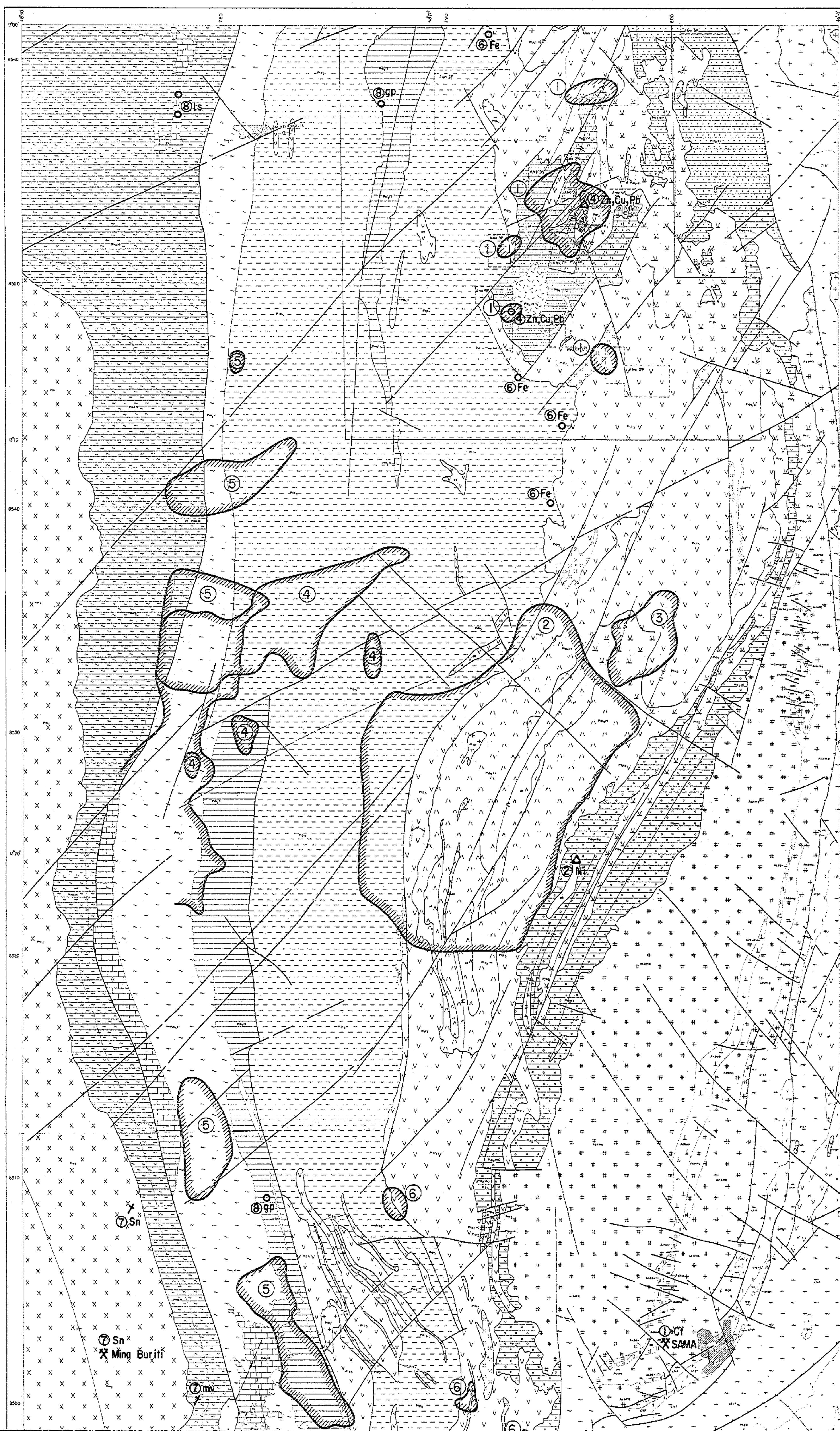

⑥ Fe
⑧ gp
⑧ ts
④ Zn,Cu,Pb
④ Zn,Cu,Pb
⑥ Fe
⑥ Fe
⑥ Fe
② Ni
⑧ gp
⑦ Sn
⑦ Sn
Mina Buriti
⑦ mv
① Cr
SAMA

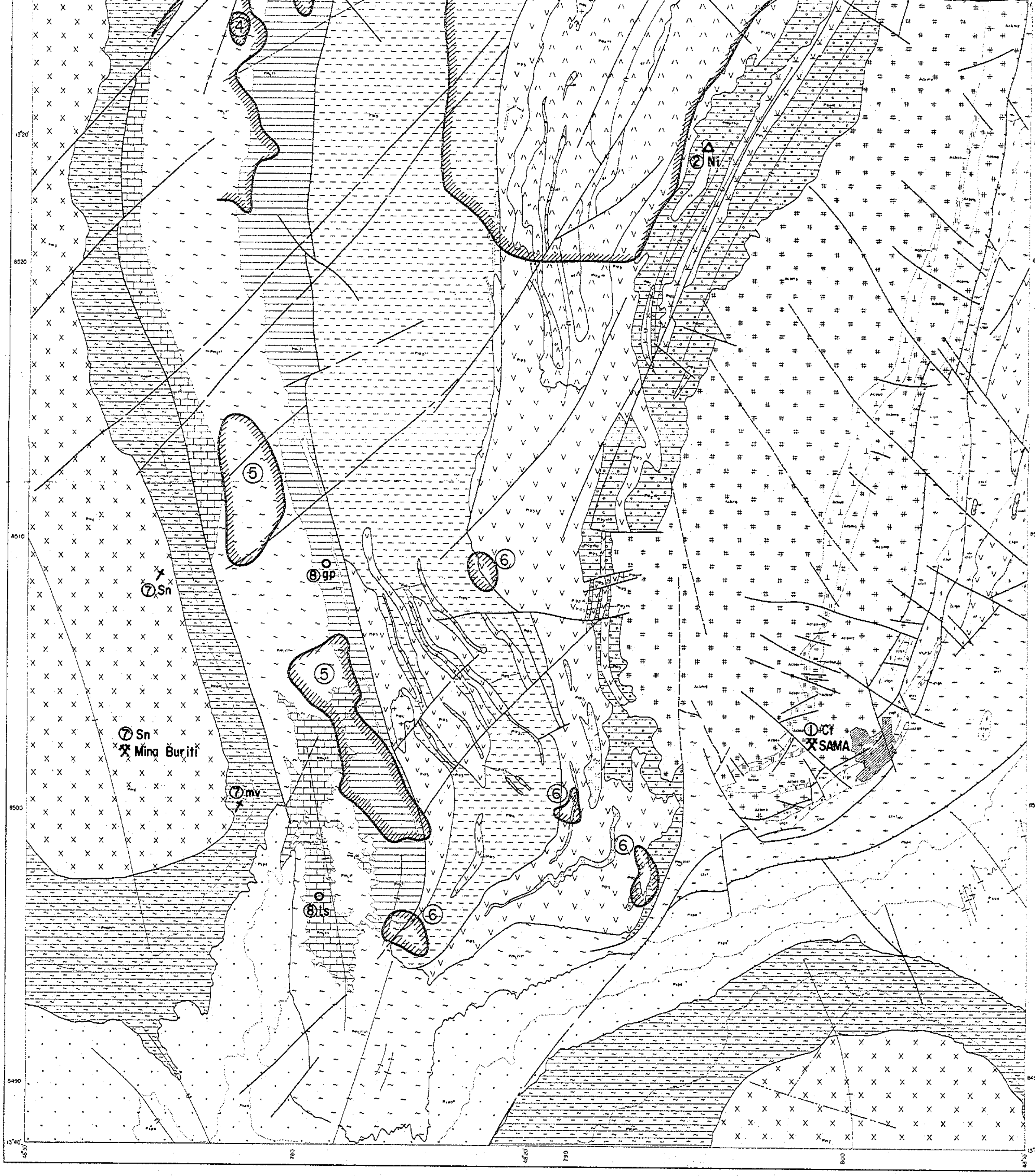

LEGEND

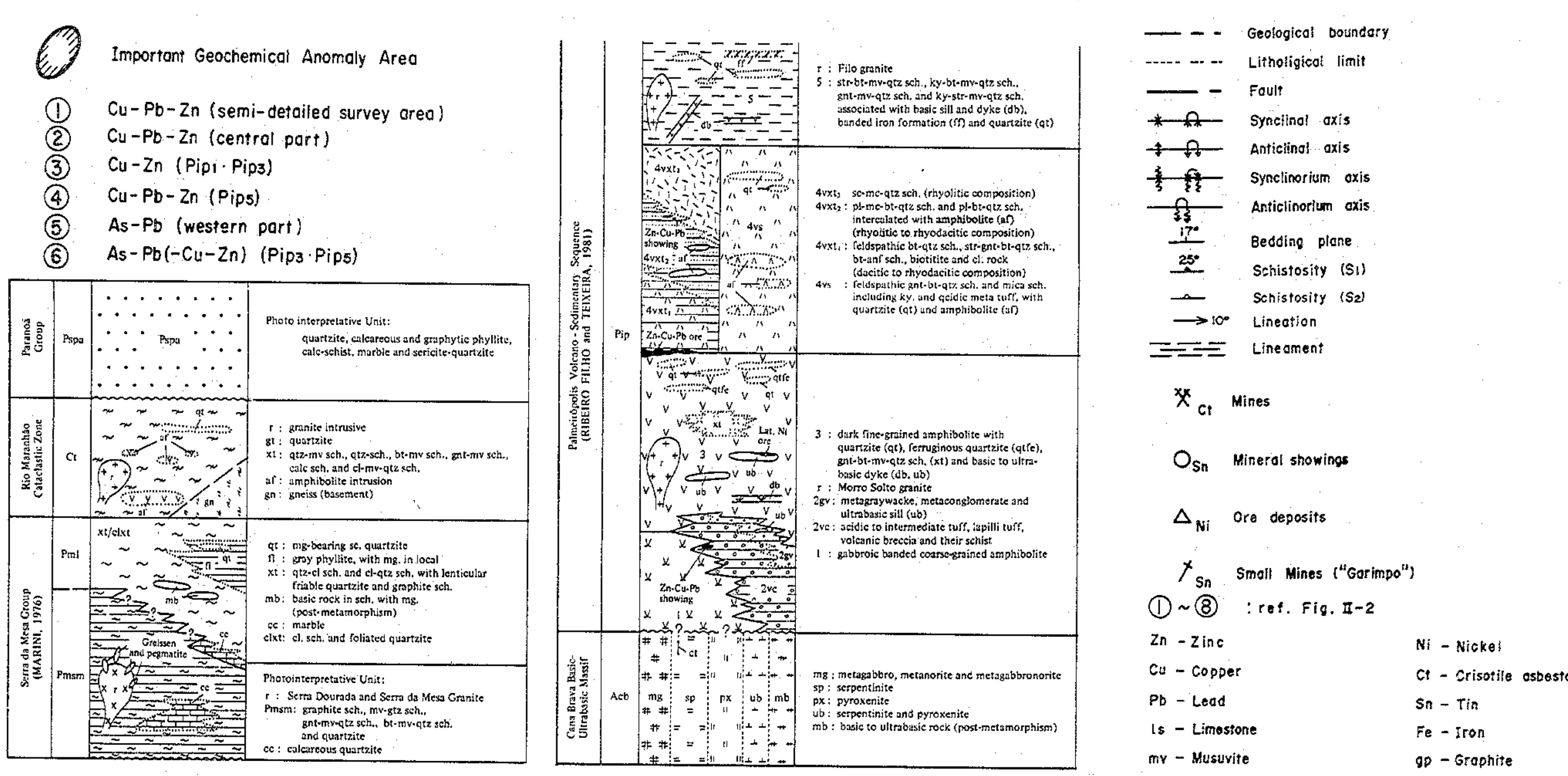

Fig. II–14 Geochemical Anomaly Map in the Surveyed Area

④ Many basic sills accompanied by dissemination of fine-grained sulfide minerals are observed in the Pip_5 formation. The anomalous zones might have been formed in this area under their influence.

⑤ This is considered to be the anomalous area caused by hydrothermal effect along fault.

⑥ This is the area overlapped with the Cu-Zn anomalies caused by leaching of Cu and Zn in the basic rocks and As anomalies affected by the hydrothermal effect along fault.

The areas described in the above items ③ to ⑥ exhibit geochemical anomalies that are different from those being aimed at. Therefore these two areas are not included in the targets of future surveys.

2–2 Geochemical Survey of Soil

2–2–1 Outline

A geochemical survey of soil (B bed) was conducted in the semi-detailed survey area ($300km^2$) selected based on the result of compilation of the existing data. Since the extent of the soil geochemical survey carried out by CPRM in the past was limited within the Alvo area, the threshold values were different in each Alvo.

The current survey was conducted for the purpose of extracting new geochemically anomalous areas by obtaining average anomalous values applicable to a broader extent.

The target components and the method of analysis were the same as those of stream sediment described in Section 2–1. As the result of analysis, the geochemically anomalous zone high in Cu, Pb and Zn was extracted immediately above the C-1 deposit. Besides, Pb and Zn zones were also extracted in the schistose rocks and at the contact between schistose rock and amphibolites at Alvo 7P, southeast of 9P, 10P, 2PA and 13P, in addition to a Cu and Zn zone at Alvo 11P.

It is worthy of note, because these are considered to be the anomalies closely associated with the mineralization similar to that of the C-1 deposit.

2–2–2 Sampling, Component of Element and Analysis Method

A map at 1:10,000 enlarged from the 1:50,000 scale drainage map was used for sampling, and the air photographs at 1:25,000 were also utilized supplementarily.

Two thousand five hundred and fifty-five soil samples were collected at the average sampling density of eight to nine samples per square kilometer (PL. II–18). The sampling was carried out along the main roads and rivers. In addition, offset survey lines were set by clearing in order to make distribution of sampling stations as even as possible through the whole area. Sample numbers, colors, constituents of soil, sampling depths and geological units were recorded at the sampling stations.

The areas sampled were divided into eight blocks with respective block numbers, and the block number of each sample was also recorded together with the sample number.

The samples collected were chemically analyzed by the atomic absorption method for the following four target components: Cu, Pb, Zn and As.

2–2–3 Data Processing

The assay results of the four components of the 2,555 samples were input into computor together with the data related to the geological units of the sampling stations (Table A–6).

(1) Single Component Analysis

Histograms and cumulative frequency distribution diagrams were made in order to extract anomalous values of each component (Figs. II–15 and 16). These diagrams are classified into the entire samples and respective lithofacies of amphibolites and schistose rocks.

The histogram for As does not show correct logarithmic normal distribution since 77 per cent of the values are below the detection limit. On the other hand, the histograms for Cu, Pb and Zn show correct logarithmic normal distribution. Although As shows a linear distribution in the cumulative frequency distribution diagram, distinct turning points were observed in most of the other three components.

Determination of anomalous threshold value was made based on the method used by Lipeltier (1964), as in the case of the stream sediment analysis. Any distict turning points in cumulative frequency distribution curve of entire samples amphiblites and schistose rocks were defined as the threshold values. If a linear distribution was shown, the points at 2.5 per cent and five per cent were respectively defined as the threshold value and the supplementary threshold value. Table II–6 shows the results.

Table II–7 shows correlation function of each component, in which Cu and Zn show a strong positive correlation, while other components hardly show any correlation.

(2) Multivariate Analysis

Two factors were extracted by factor analysis in the same manner as in the case of the stream sediment analysis (Table II–8). The first factor is Cu-Zn, and the second factor Pb-As.

2–2–4 Results of Interpretation

(1) Single Component Analysis

The anomalous values of each component obtained in the data processing stage were plotted

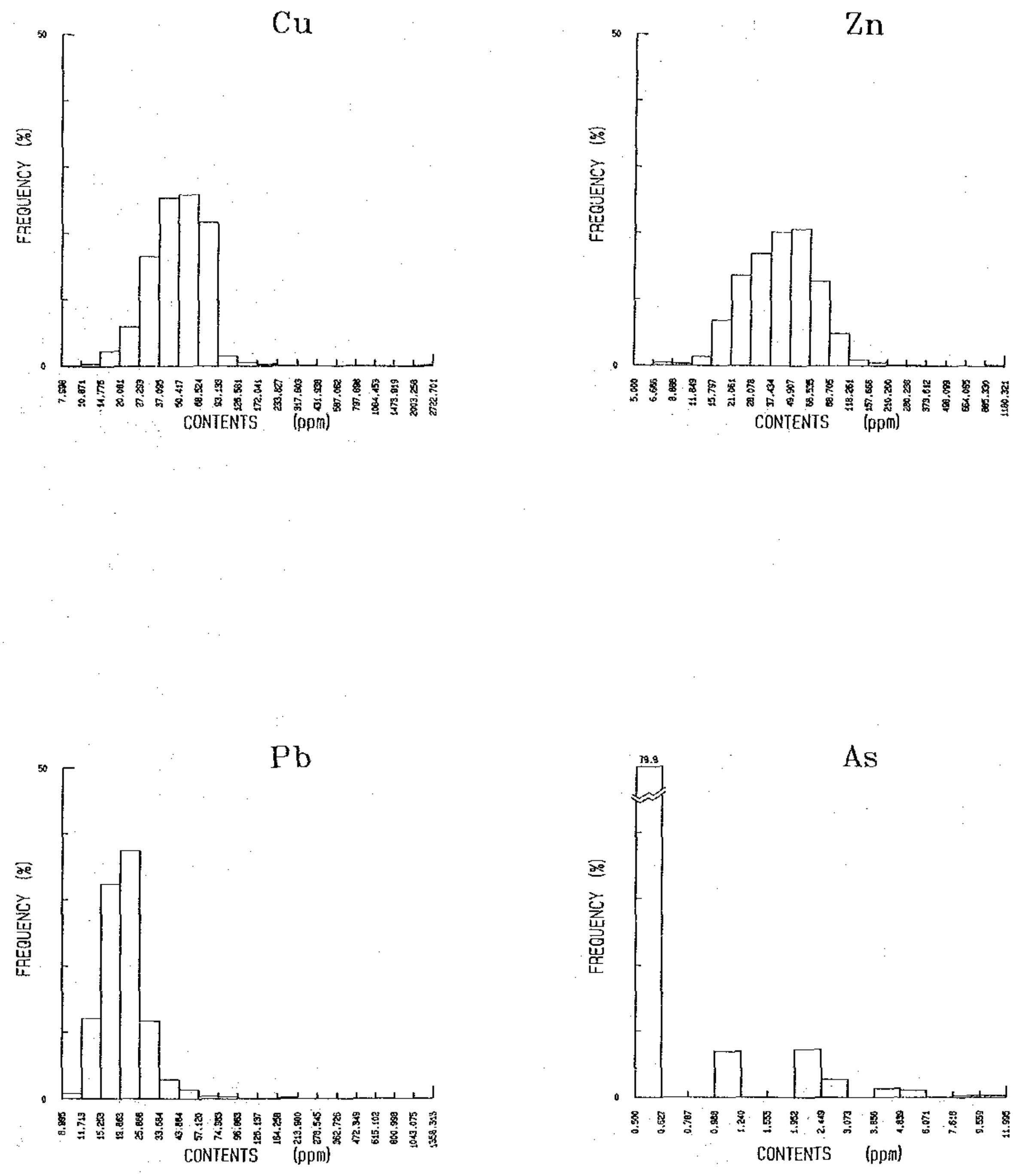

Fig. II–15 Histogram for Cu, Pb, Zn and As of Soil (1)

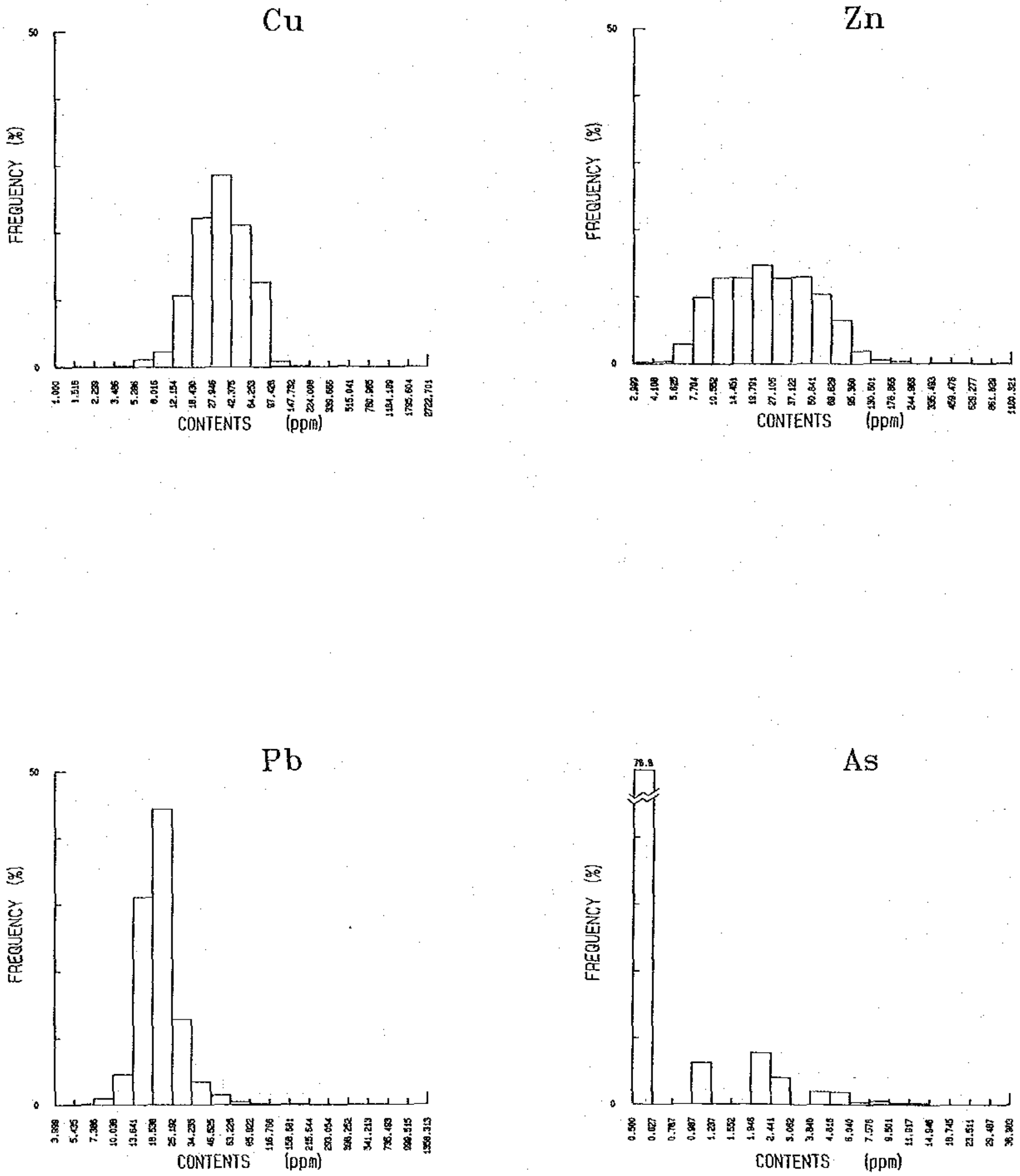

Fig. II–15 Histogram for Cu, Pb, Zn and As of Soil (2)

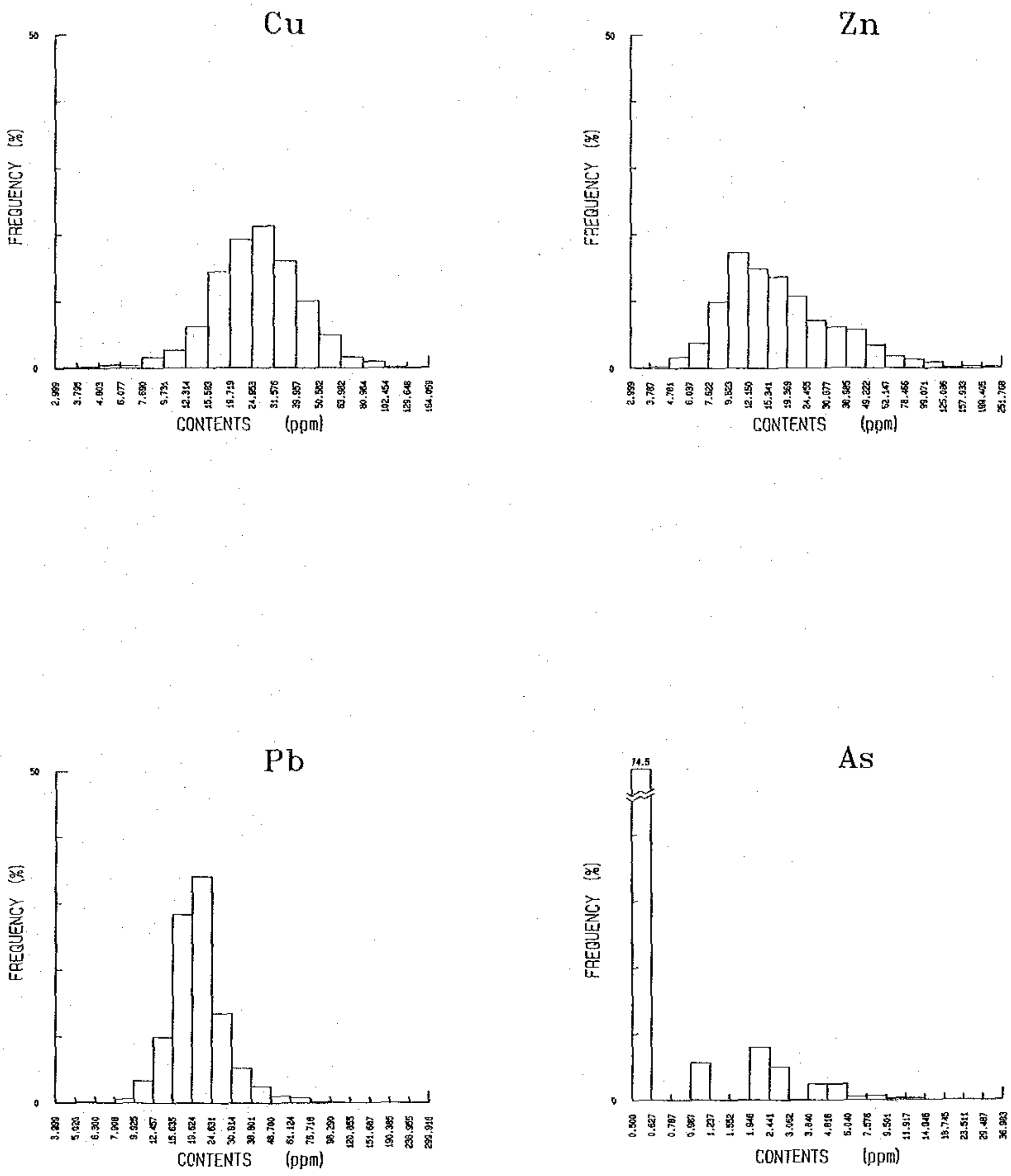

Fig. II–15 Histogram for Cu, Pb, Zn and As of Soil (3)

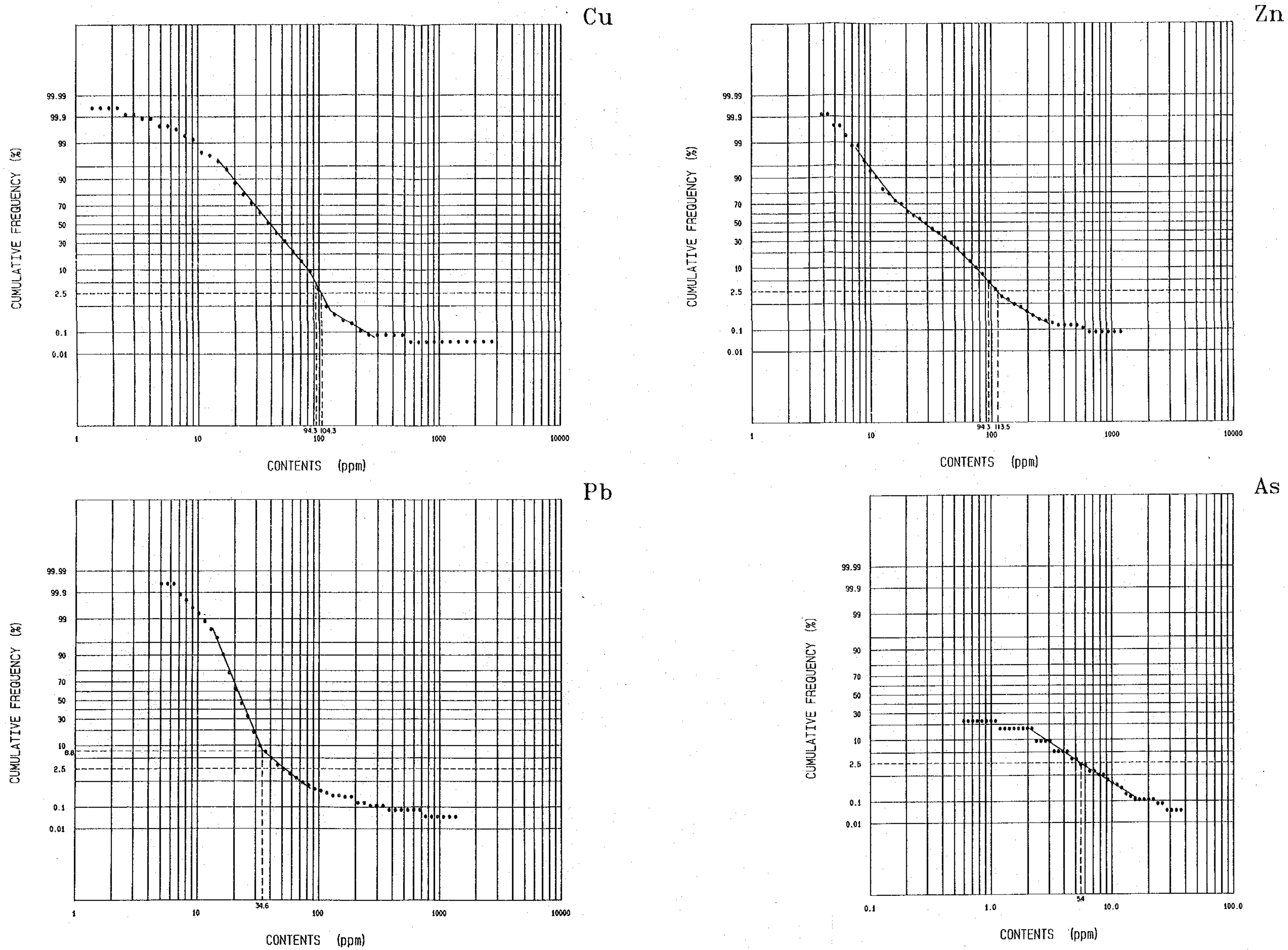

Fig. II–16 Cumulative Frequency Distribution of Cu, Pb, Zn and As of Soil (1)

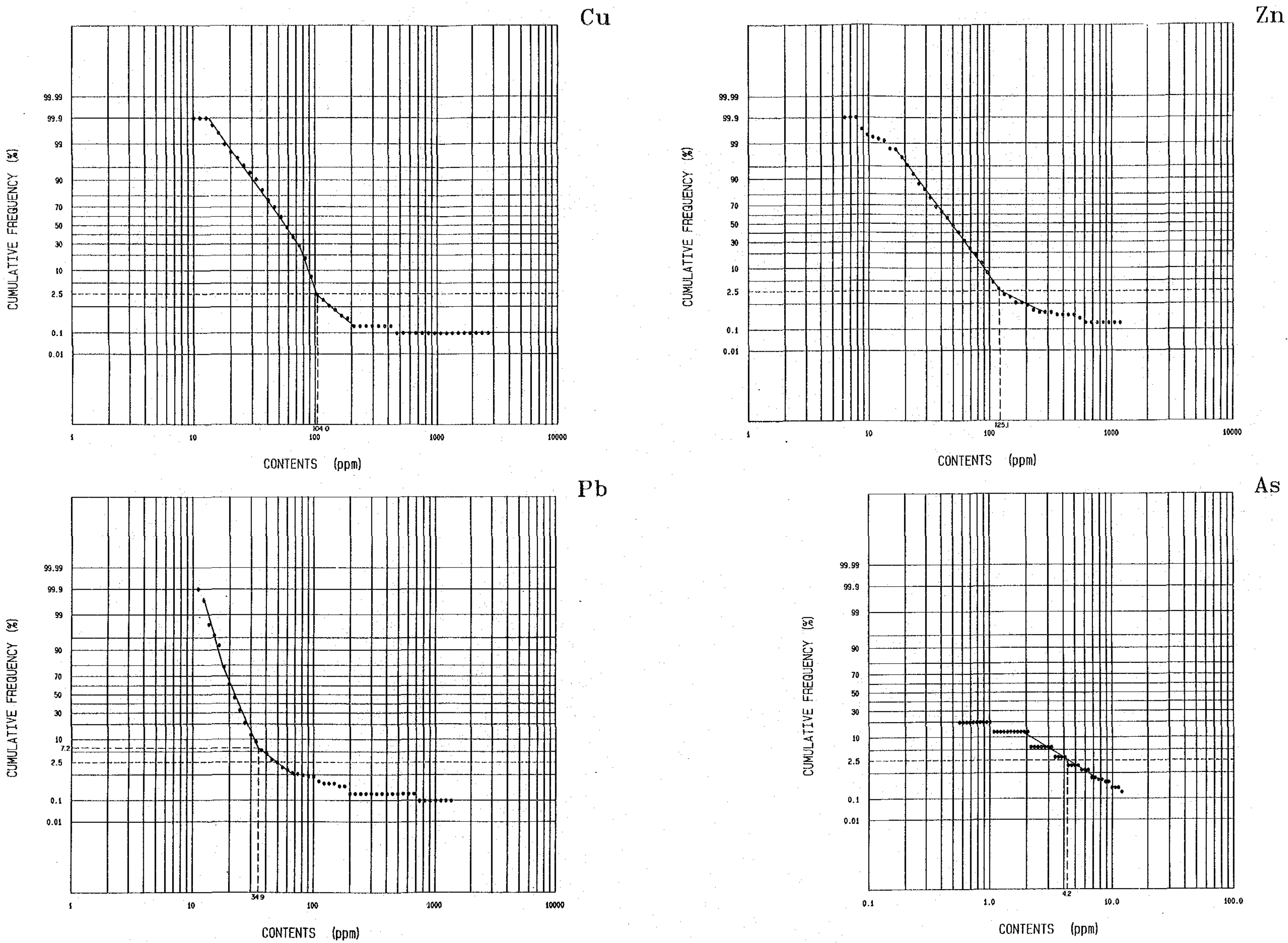

Fig. II–16 Comulative Frequency Distribution of Cu, Pb, Zn and As of Soil (2)

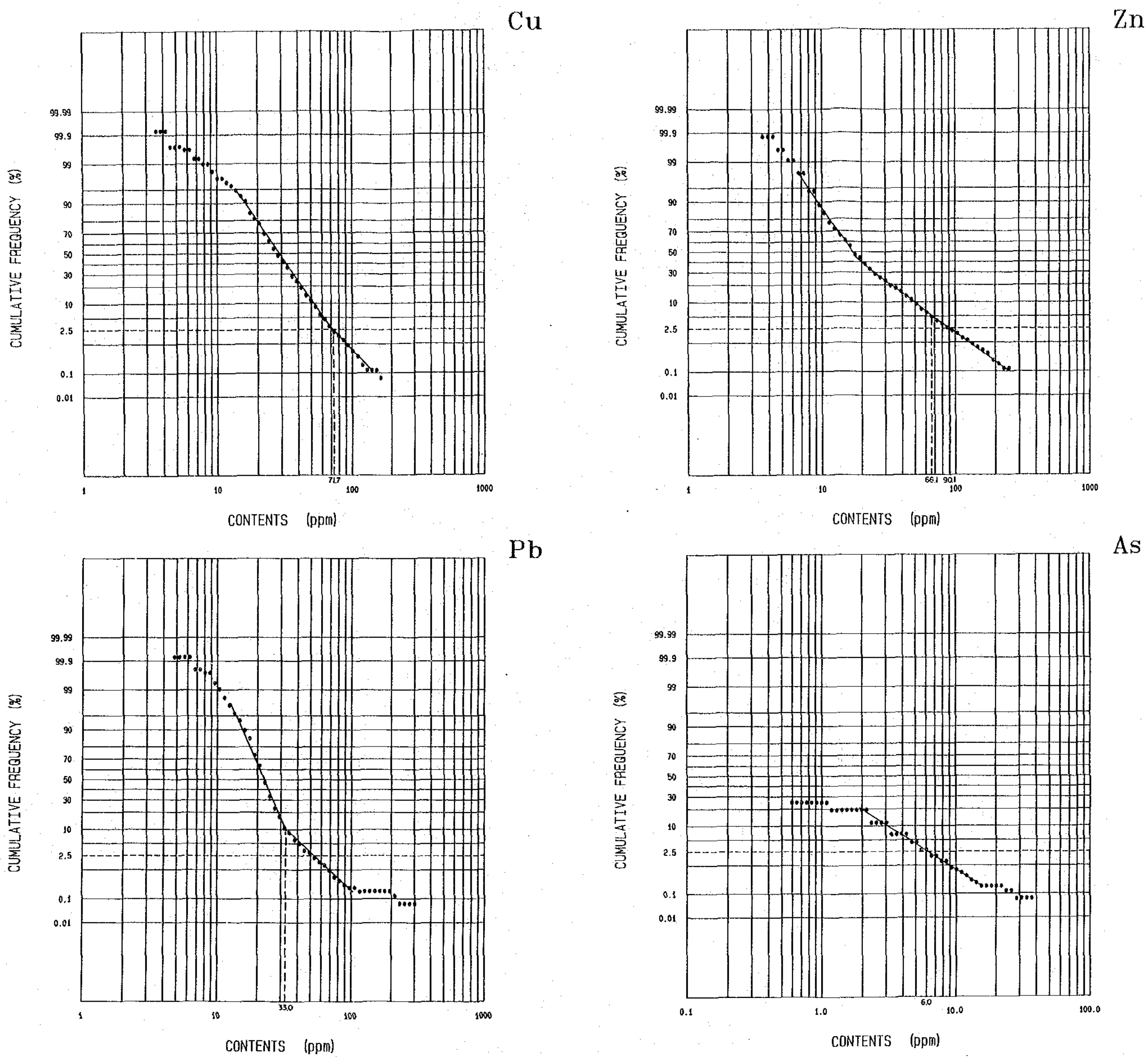

Fig. II–16 Comulative Frequency Distribution of Cu, Pb, Zn and As of Soil (3)

Table II–6 Results of Simplified Statistical Treatment Geochemical Data of Soil Samples

Element	Lithology	Max. (ppm)	Min. (ppm)	Mean (ppm)	t' (5%) (ppm)	t (2.5%) (ppm)
Cu	Total	2,720	5 (1)	33,413	94.3	104.3
	Amphibolite	2,720	8	49,476	–	104.0(2.5%)
	Schist	164	5 (3)	26,011	–	71.7(2.5%)
Pb	Total	1,358	5 (4)	20,785	–	34.6(8.8%)
	Amphibolite	1,358	9	20,817	–	34.9(7.2%)
	Schist	300	5 (4)	20,835	–	33.0(10%)
Zn	Total	1,180	5 (3)	25,403	94.3	113.5
	Amphibolite	1,180	5	42,939	–	125.1(2.5%)
	Schist	252	5 (3)	17,824	66.1	90.1
As	Total	37	1 (0.5)	–	–	(5.4)
	Amphibolite	12	1 (0.5)	–	–	(4.2)
	Schist	37	1 (0.5)	–	–	(6.0)

Table II–7 Correlation Matrix of Four Elements of Geochemical Data of Soil Samples

	Cu	Pb	Zn	As
Cu	1.000			
Pb	0.220	1.000		
Zn	0.697	0.223	1.000	
As	0.011	0.217	–0.047	1.000

Table II–8 Results of Factor Analysis of Geochemical Data of Soil Samples

Factor Loadings (varimax rotation)			Communality
Element \ Factor No.	Factor 1	Factor 2	
Cu	0.824	0.121	0.6938
Pb	0.216	0.443	0.2428
Zn	0.837	0.055	0.7035
As	–0.069	0.480	0.2353
Factor contributions	80.326%	21.932%	

on the 1:20,000 drainage map enlarged from the original scale of 1:50,000 (PL. II–19 to 26).

Because content levels of each component are different according to the lithofacies, the analysis was performed, in addition to the analysis of the entire samples, by dividing the soils into the one derived from basic rocks and the other derived from achistose rocks.

1) Copper (Cu)

The threashold value (t) and the supplementary threshold value (t') of the whole sample are 105 ppm and 95 ppm respectively. PL II–19 indicates contour lines of 40 ppm, 80ppm, 95 ppm (t'), and 105 ppm (t). Their respective cumulative frequencies are approximately 50%, 10%, 5% and 2.5%.

Copper anomaly zones were extracted in the vicinity of the C-1 ore body, as well as at Alvo 1P, 3P, 2PA, 11P, in the southeast of 11P and in the southeast of the semi-detailed survey area.

In the meantime, the analysis by respective lithofacies indicates, that the threshold value of the soil derived from basic rocks is 104.0 ppm, and that of the soil derived from schistose rocks is 71.7 ppm. Compared with the analysis of the entire samples, more anomalous zones were found in the soil derived from schistose rocks (PL II–23).

In the analysis by lithofacies copper anomaly was extracted most widely and strongly immediately above the C-1 ore deposit. In addition, Cu anomalies were extracted in a slightly concentrated manner to the south of Alvo 2PA and Alvo 6P among the extent of distribution of the Pip_4vxt_1 member which is the host rock of the C-1 deposit. These anomalies, however, are not so strong as the one immediately above the C-1 deposit.

Cu anomalies were also extracted in the Pip_5 formation in Alvo 3P, in schist in Alvo 11P and the east of it, and in the Pip_5 formation to the southwest of Alvo 11P. The schist to the east of Alvo 11P and the one in the Pip_5 formation to the southwest of Alvo 11P closely resemble the Pip_4vxt_1 member. Especially because gossan has been confirmed in the Pip_5 formation, it will be necessary to examine the geology in the surrounding areas of these parts.

Besides the above, Cu anomalies were also extracted in the Pip_3 formation in the southeastern part of Morro Solto, in the Pip_3 formation to the east of Alvo 12P and in the surrounding part of the basic sill in the Pip_5 formation in the northeastern part of the semi-detailed survey area. All of these however are considered to have reflected the characteristic of the country rocks.

2) Lead (Pb)

The threshold value (t) of the whole samples is 35 ppm (8.8%), and PL II–20 also indicates contour lines of 20 ppm (65%) and 30 ppm (18%).

The difference of threshold values by lithofacies is not great as compared with the case of copper, and that of the soil derived from basic rocks is 34.9 ppm and that derived from schistose rocks 33.3 ppm.

The largest zone, among other lead anomalous zones, spreads over the area from immediately above the C-1 ore deposit to Alvo 2P, 7P through 13P.

In the Pip_4 formation, additional Pb anomalies were extracted, in Alvo 2PA and the north of it, in Alvo 9P and Alvo 10P and the east of it (PL II–20, 24).

Small anomalies are also scattered in the Pip_2 and Pip_5 formations.

3) **Zinc (Zn)**

The threshold value (t) and the supplemental threshold value (t') of the whole samples are 114 ppm and 95 ppm respectively. PL II–21 indicates contour lines of 20 ppm, 75 ppm, 95 ppm (t') and 114 ppm (t). Their respective cumulative frequencies are approximately 63%, 10%, 5% and 2.5%.

Copper anomaly zones were extracted in the area immediately above the C-1 ore body, as well as at Alvo 1P, 3P, 2P-13P, 7P, 9P, 10P, 11-12P and in the southeast of the semi-detailed survey area.

The threshold values vary greatly by lithofacies in the same way as in the case of copper. The values are 125.1 ppm in the soil derived from basic rocks and 90.1 ppm in that derived from schistose rocks.

Compared with the analysis of the whole samples, part of the anomalies has not been found in the soil derived from basic rocks and an additional anomaly zone was detected in the soil derived from schistose rocks.

In the analysis by lithofacies the zinc anomalous zones were extracted at four places in a direction from NE to SW, starting immediately above the C-1 ore deposit to Alvo 7P, through 9P and 10P. Besides these, small anomalies were also detected at Alvo 2PA, 13P, 12P and in the south of 6P, all of which are distributed in the schistose rocks and in amphibolite around the schistose rocks (PL II–25). Small anomalies are also scattered in the Pip_3 formation in the southeastern part of Morro Solto and in other soil derived from basic rocks, but they do not show favorable concentration.

4) **Arsenic (As)**

The threshold values of arsenic were determined at 5.4 ppm for all the samples while they are 4.2 ppm in the soil derived from basic rocks and 6.0 ppm in that derived from schistose rocks. Since the assay values of arsenic are as small as 12 ppm at the maximum in the soil derived from the basic rocks and 37 ppm at the maximum in the soil derived from schistose rocks, it is appropriate to define these values as high concentration values rather than anomalous values.

The zones of high concentration of arsenic extend continually along the fault of N-S system in the Pip_5 formation and the Pm_1fl member in the western periphery of the semi-detailed survey area (PL II–22, 26).

Besides the above, additional high concentration values are also scattered mainly in the schistose rocks in the Pip_4 and Pip_5 formations.

(2) Multivariate Analysis

PL. II–27 and 28 show analysis diagrams of the first and second factors.

1) First Factor (Zn-Cu)

Moderate to high factor contribution zone obtained in the same manner as that of the stream sediment analysis was extracted extensively on the east of longitude 790 in a concentrated form. The zone includes all the anomalies of copper and zinc obtained by the single component analysis, as well as all the Alvos. It is also consistent with the distribution of the Pip_1 and Pip_3 formations in the eastern part.

Although high factor concentration zones are scattered in the Pip_5 formation in the western part, their distribution is confined to the basic sills and their surroundings.

As mentioned above, the factors are roughly divided into the one characterizing the Cu-Zn mineralization and the other reflecting the characteristic of the country rock.

2) Second Factor (As-Pb)

The largest zone of moderate to high factor contribution was extracted in the same zone as that of arsenic in the western peripheral part of the semi-detailed survey area.

Some moderate to high factor contribution zones were extracted in a concentrated form at Alvo 2P, north of Alvo 2PA, Alvo 9P to 7P through east of 7P, west of 13P and Alvo 10P to east of 10P.

In addition, several zones are also scattered in the Pip_2 formation distributed from the north to the south of the eastern end of the area and in the Pip_3 formation distributed to the northeast and in the southern part of Alvo 12P.

It is thought that the geochemical anomalies which give high factor contribution are the reflection of the hydrothermal effect ascended along the fault.

Since it is unclear whether the anomalies scattered in schistose rocks in the semi-detailed survey area is caused by mineralization of the C-1 deposit type or it is the indication of the characteristic of the schistose rocks, future investigation would have to be required.

2–2–5 Relation between Geochemical Anomaly and Mineralization

While many geochemically anomalous zones were extracted as the result of single component analysis and multivariate analysis, the investigation on the relation between these anomalous zones and mineralization resulted in extracting the geochemically anomalous areas of importance, such as two Cu-Pb-Zn zones, nine Pb-Zn zones, six Cu-Zn zones and four Cu-Pb zones (PL. II–29 and Fig. II–17). For these zones, the following remarks are to be noted:

① Cu-Pb-Zn Zones

The zones were extracted immediately above the C-1 deposit and in Alvo 2PA.

② Pb-Zn Zones

Some concentrated zones were extracted in each of Alvo 7P, Alvo 9P and Alvo 10P, and others are scattered in the surrounding areas of Alvo 2PA and Alvo 13P. All these are consistent with the distribution of schistose rocks.

③ Cu-Zn Zones

Although the six anomalies extracted are small in scale, five of these are associated with schistose rocks and occurrence of gossan has been confirmed in some of them.

④ Cu-Pb Zones

Each of the two zones was extracted in the Pip_3 and Pip_5 formations respectively.

Among those described above, the Cu-Pb-Zn zones and the Pb-Zn zones, as well as the Cu-Zn zones which are consistent with the distribution of schistose rocks, are considered promising ones to be associated with mineralization.

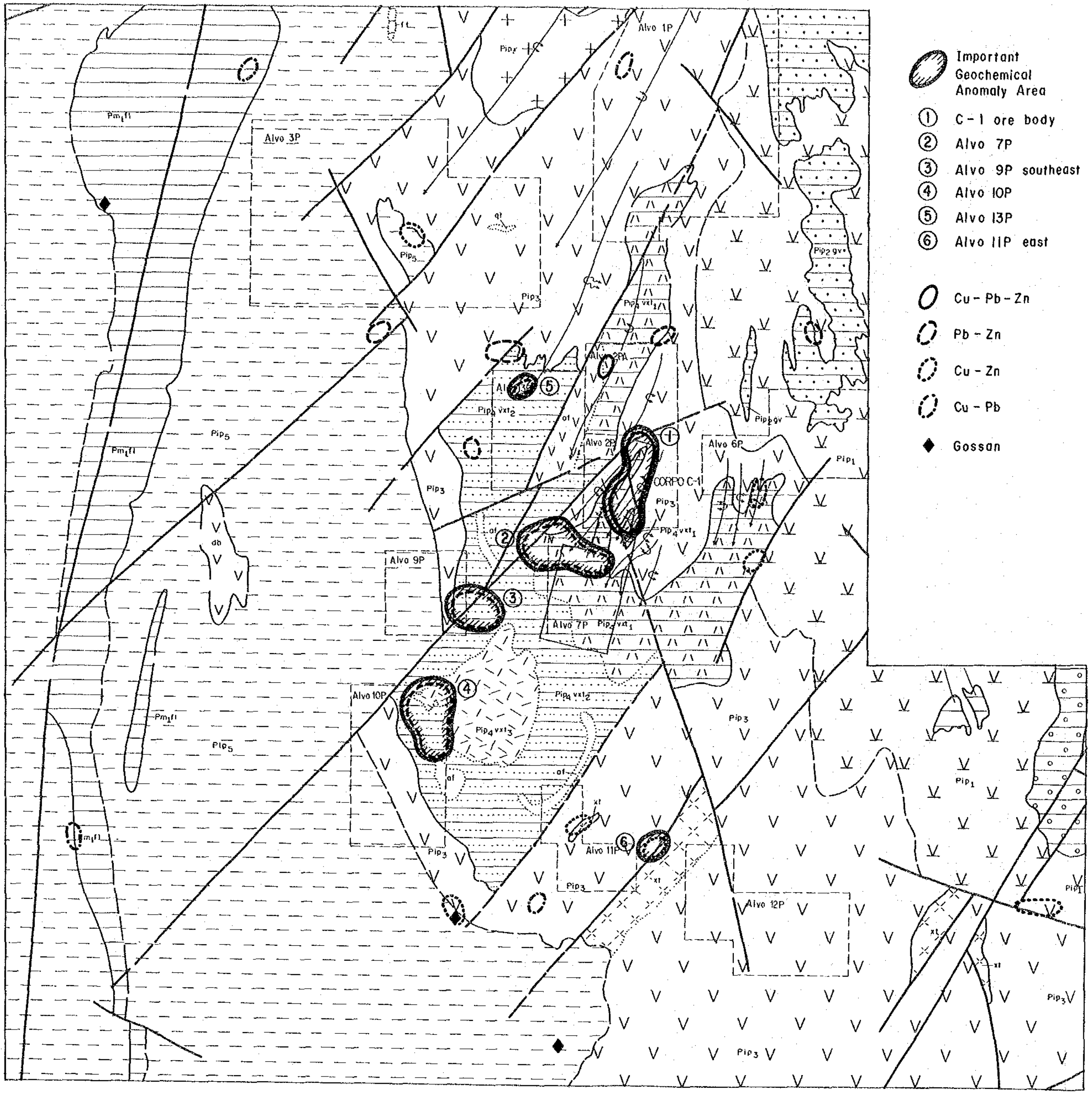

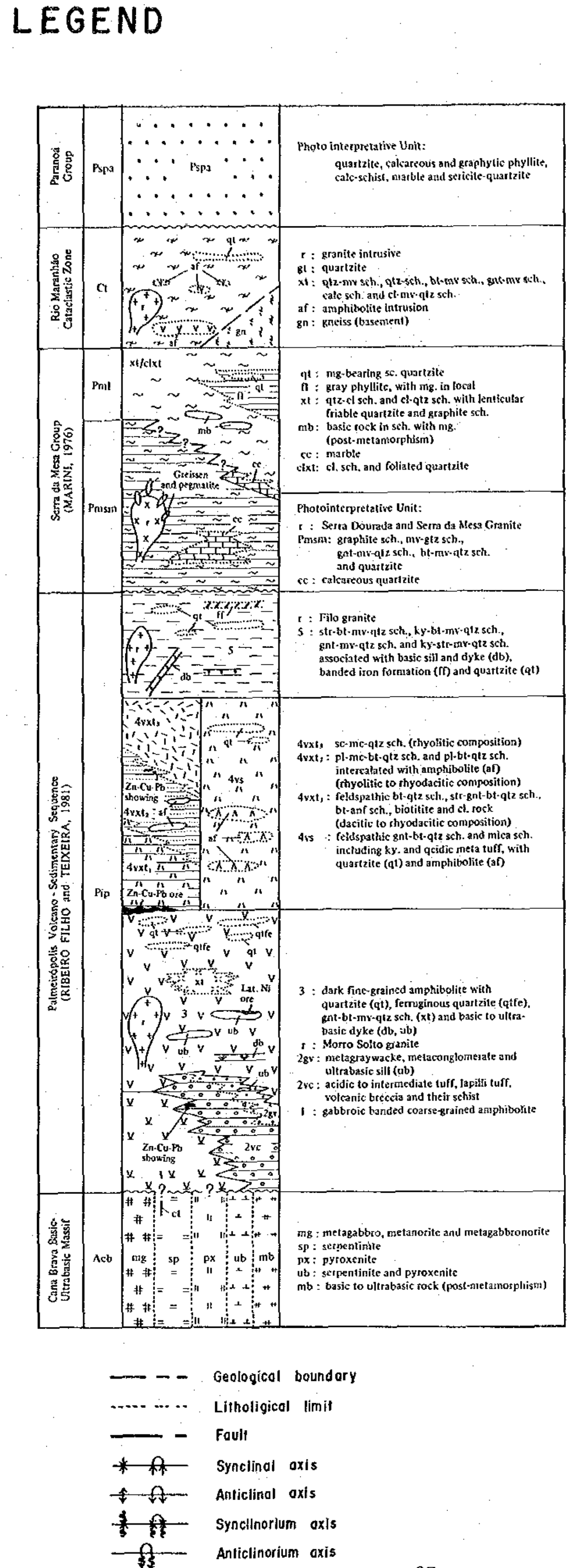

Fig. II–17 Geochemical Anomaly Map in the Semi-detailed Area

III GEOPHYSICAL SURVEY

CHAPTER 1 OUTLINE OF SURVEY

In order to investigate deeply the geology of the area, two geophysical techniques based on the electrical response of the geological structure were carried out: CSAMT (Controlled-Source Audio Magneto-Telluric) and SIP (Spectral Induced Polarization) methods.

The CSAMT method permitted us to delineate the resistivity distribution to select the most promising potential area for mining exploitation. After a preliminary analysis of the above-mentioned survey, a SIP survey were carried out to further clarify the electrical response of the C-1 ore deposit.

The flat topography of the survey area permitted to easily access the proposed survey lines and points. The surveyed area is indicated in Fig. III-1.

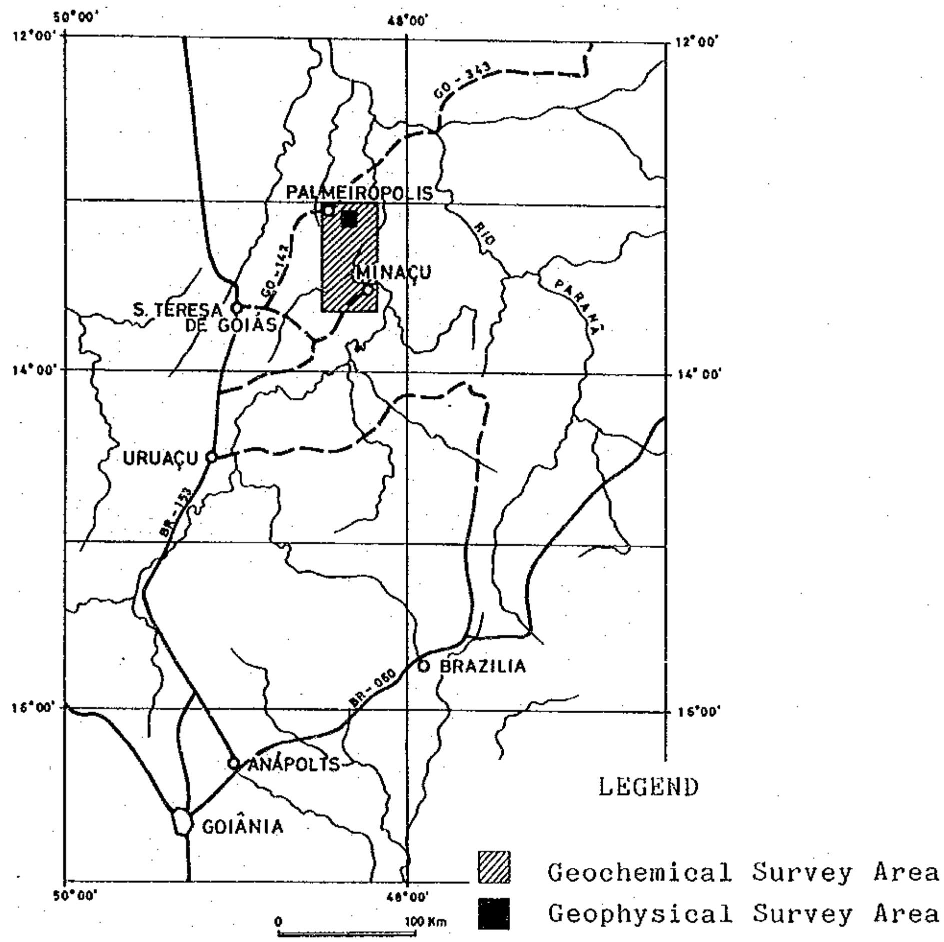

Fig. III-1 Location Map of Survey Area

CHAPTER 2 CSAMT METHOD

Based on the existing geological, geochemical and geophysical information of the area, it was thought that the CSAMT technique would provide us with clear answers to the electrical behaviour of the structure under study.

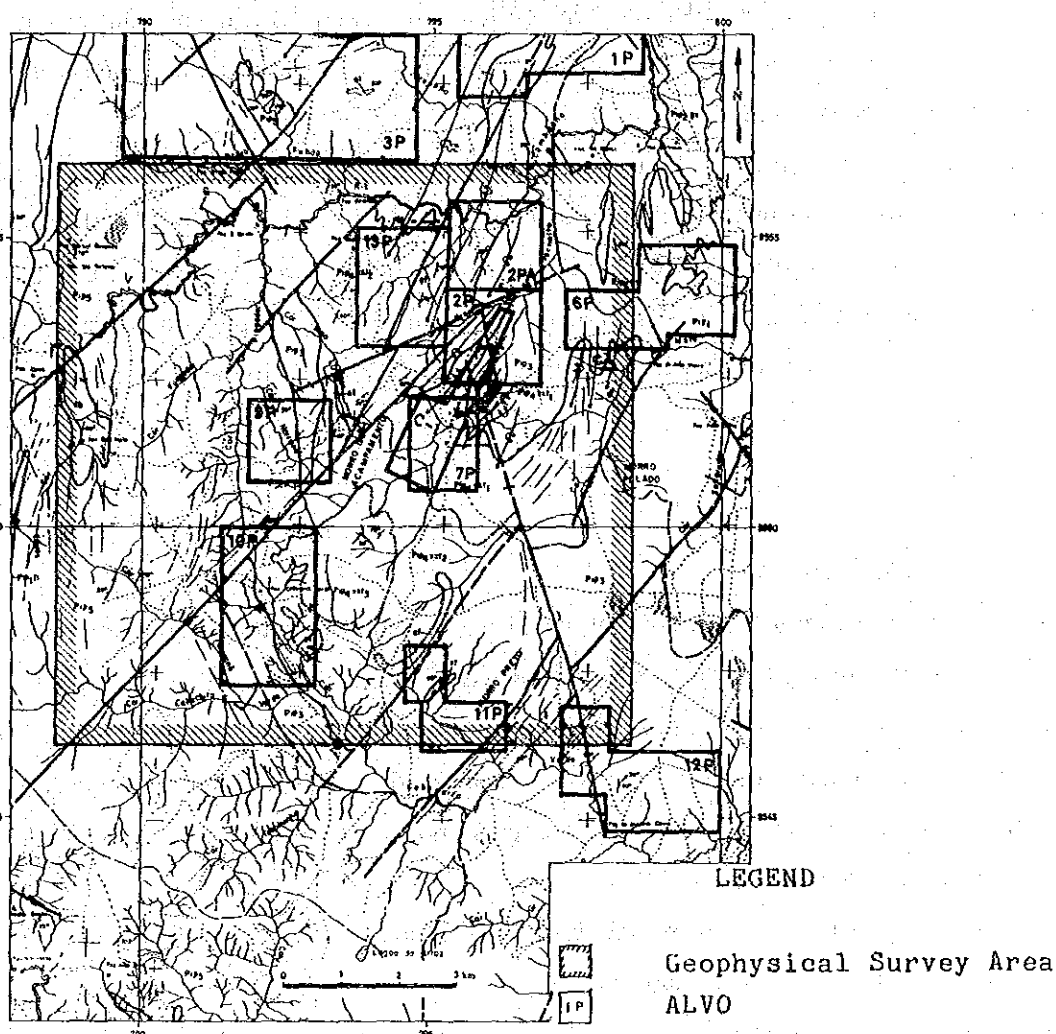

Fig. III－2 Location Map of Geophysical Survey Area

2–1 Survey Methods

This electromagnetic exploration technique recently developed has allowed the geophysicists to overcome the low magnitude and variability of the natural signals in the Magneto-Telluric (MT) method by applying a controlled current through a long grounded wire. As in the MT method, the depth of penetration of the electromagnetic waves are a function of the earth resistivity and of the frequency of the applied waves and expressed as the following equation:

$$d = 503\sqrt{\rho/f}$$

In this equation, d is called the skin depth in meters and defined when the magnitude of the electromagnetic field becomes 1/e (about 37%) of that of the surface. ρ is the resistivity in Ωm and f is the frequency in Hz.

From this equation, it can be seen that the low frequencies utilized in the CSAMT can penetrate into greater depths, allowing us to investigate deep information. Furthermore, by this technique, the measuring of the electric and magnetic fields accross a range of frequencies lead to the determination of the resistivity as a function of the depth. The relation between the apparent resistivity ρ_a, the electric field E, the magnetic field H, and the frequency f is given by the well-known Cagniard Equation:

$$\rho = \frac{1}{5f}\left(\frac{E}{H}\right)^2$$

2–1–1 Field Procedure

In order to conduct a better analysis and interpretation of the information collected, such as for instance, analysis of the apparent resistivity sections and modeling determinations, about 2/3 of the CSAMT stations were set along the designed survey lines. The remaining stations were spread equally among the lines. However, the exact locations and intervals between them were determined in the field by means of compass and measurement tapes and related to a base point located at the Campsite (CPRM).

In relation to the current source, it was placed in such a way that the dipole transmitter be placed a far enough distance from the stations so as to detect the electromagnetic fields as nearly plane waves at the receiver. In theory, it is necessary that the stations should be away from the source within a distance no closer than 3 times the skin depth defined above. If for some reasons, such as for instance, the high resistivity of the ground, the plane wave condition can not be met, then "near field" corrections affecting mainly the deeper information, has to be made.

At the stations, the length of the potential dipole used was 50m and oriented parallel to the transmitter dipole. In ocassions, to decrease the underground resistance higher than 20 KΩ, more water were placed to the ground surrounding the porous pots.

The magnetic field was detected by an AMT antenna coil oriented perpendicular to the electric dipole. The received information was then fed to a digital processor which calculates the apparent resistivity by using the Cagniard Equation mentioned before. The data so calculated is then printed and stored in a cassete printer incorporated to the receiver. The following example gives an example of the data stored in the casette tape.

ST	: Station Number
FREQ	: Frequency Code
GAINS	: Gain in the Receiver
FILTER	: Notch Filter (01 = on)
STACKS	: Stacking Times
A-SP	: a-Spacing
COIL	: Coil Channel
GAINS1	: Gain of the coil
ME	: Measured Potential (V)
PE	: E Phase (rad)
MH	: Magnitude of H (V)
PH	: E Phase (rad)
E	: E-Field (mV)
H	: H-Field (mV/gamma)
RHO	: Resistivity (Ωm)
PD	: Phase Difference (PE-PH)
CK	: Coil Factor

```
***** 0017
ST 0192 FR006 4 HZ CSAMT
GAINS 13 13 FILTER 00 STKS 0277
A-SP050. COIL 1 GAINS1 CRNT 05.9
 ME+.1171113E-4  PE+.7963354E-1
 MH+.1874730E-4  PH-.4316468E+0
  E+.2342221E-6   H-.2331752E-4
RHO+.5045001E+1  PD+.5102001E+0
 CK+.8840003E+0

***** 0018
ST 0192 FR006 4 HZ CSAMT
GAINS 13 13 FILTER 00 STKS 0265
A-SP050. COIL 1 GAINS1 CRNT 05.9
 ME+.1873535E-4  PE+.1149625E+0
 MH+.1679700E-4  PH-.4240708E+0
  E+.2147067E-6   H+.2009170E-4
RHO+.5200935E+1  PD+.3891086E+0
 CK+.8048883E+0
```

In this survey, 10 frequencies were used in the AMT range, namely, 4,8,16,32,64,128,256, 512,1,024 and 2,048 Hz. Apparent resistivities curves such as those illustrated in Fig. III-3, are made by plotting in a log-log scale, the values of apparent resistivity for every frequency.

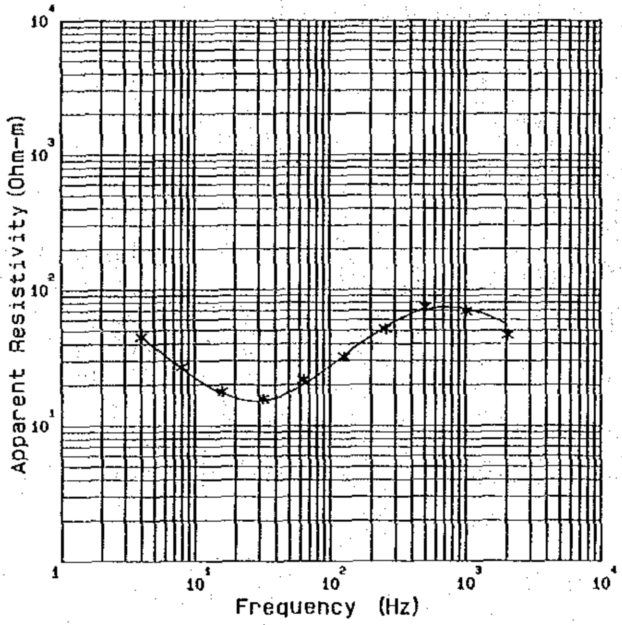

Fig. III−3 ρa-f Curve

The logistic for the CSAMT survey utilized is illustrated in the Fig. III-5, and the specifications and survey amounts are shown in the table III−1.

Table III−1. Specification and Survey Amounts for CSAMT Survey

Area Covered	Station Spacing	Current Electrode Separation	Number of Stations
100 Sq · km	400 − 500 m	T x 1 1900 m	56
(10km x 10km)		T x 2 2000 m	42 Total
		T x 3 1800 m	65 202
		T x 4 2000 m	39

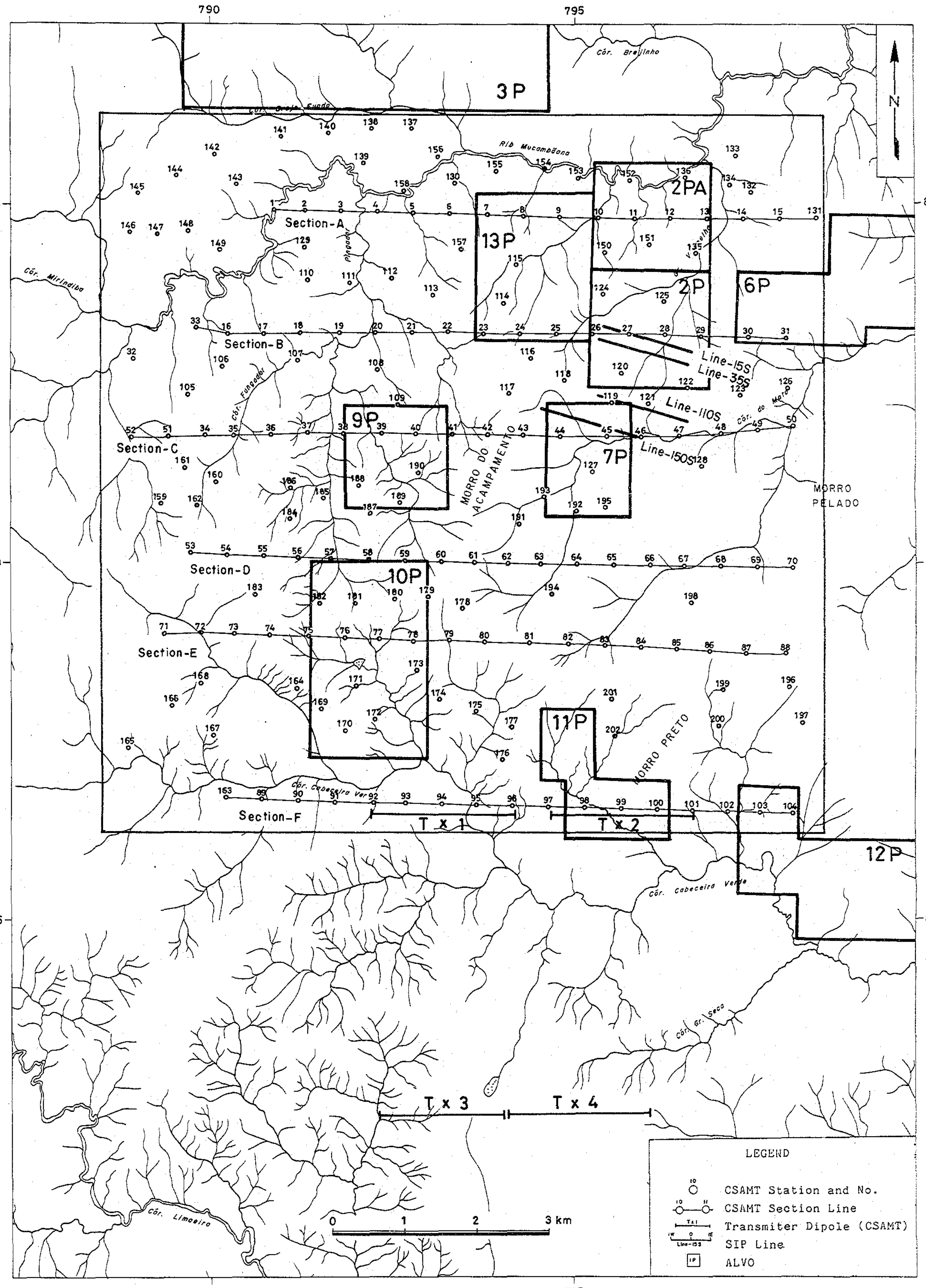

Fig. Ⅲ–4 Location Map of the CSAMT Survey

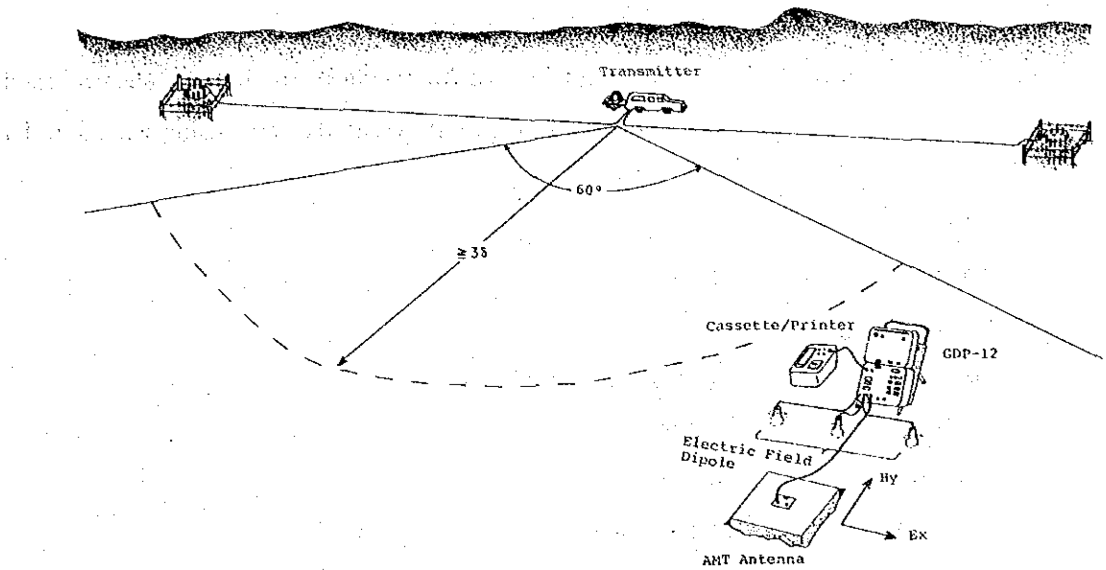

Fig. III−5　Logistics of CSAMT Survey

2−1−2　Instrumentation

The survey was carried out using an equipment manufactured by Zonge Engineering & Research Organization, Inc. (U.S.A.) which permitted to measure the electric field and the magnetic field as well as their phase differences for every frequency.

The instrumentation used were as follows:

1) Transmitter System

a) Engine generator (ZMG-20)

Output 20KVA, 3200RPM, 400Hz

b) Transmitter (GGT-25)

Maximum output	25KW
Output current	0.2−20 A
Maximum output voltage	1KV
Frequency	DC−12KHz

c) Transmitter Controller (XMT-2)

Frequency range	1/16−2048Hz

2) Receiver System (2 sets)

a) Data processor (GDP-12/2 GB)

Frequency range	1/16−2048Hz
A/D converter	12 bit with the built-in computer, boot ROM, 16Kbyte RAM, and 50/60Hz notch filter

Input voltage	Minimum 0.2 μV/1024 stacking
Output	Station number, stacking times, frequency, electric field, magnetic field, apparent resistivity, etc. using RS-232C I/F to CAP-12
Size	36.1 x 31.8 x 24.2 cm
Weight	15 kg

b) Casette Printer (CAP-12)

Size	29.8 x 23.9 x 20.5 cm.
Weight	9.8 kg
Interface	RS-232C
R/W Speed	2,400 baud

Casette tape (minicasette)

8000 kbit,	100–400 data block stored

Printer

Electric discharge printer

Writing speed	50–170 mm/sec.

c) Antenna Coil

2 axes ferrite coil

Coil sensitivity	0.2 mV/γ/Hz
Size	40.4 x 40.7 x 8.9 cm
Weight	9.8 kg

2–2 Data Analysis

Since in general the earth is not homogeneous, the apparent resistivity obtained for each frequency at each station does not represent the true resistivity of the geological structure under investigation. Therefore, to better analyze the information, a one-dimensional analysis is first carried out by assuming the multi-layer structure.

To begin with, a theoretical curve is to be matched by trial and error techniques to the observed data, by using assumed parameters such as number of layers, thickness and resistivities of every layer.

Using the above results as initial values, a least square iteration technique is utilized to determine the most suitable model. In these calculations, the apparent resistivity is calculated according to the equation:

$$\rho = -i \frac{Z^2}{\omega\mu}$$

where, Z = wave impedance

ω = angular frequency

μ = magnetic permeability

For the 3-layer case, Z is given by

$$Z = \frac{i\omega\mu}{r_1} \coth \left[r_1 h_1 + \coth^{-1} \frac{r_1}{r_2} \left(\coth \left(r_1 h_2 + \coth^{-1} \frac{r_2}{r_3} \right)\right) \right]$$

where, $r_i = \frac{i\omega\mu}{\rho i}$

hi = thickness of i-th layer

ρi = resistivity of i-th layer

As a simple example, a chart for a 2-layer case is illustrated as follows:

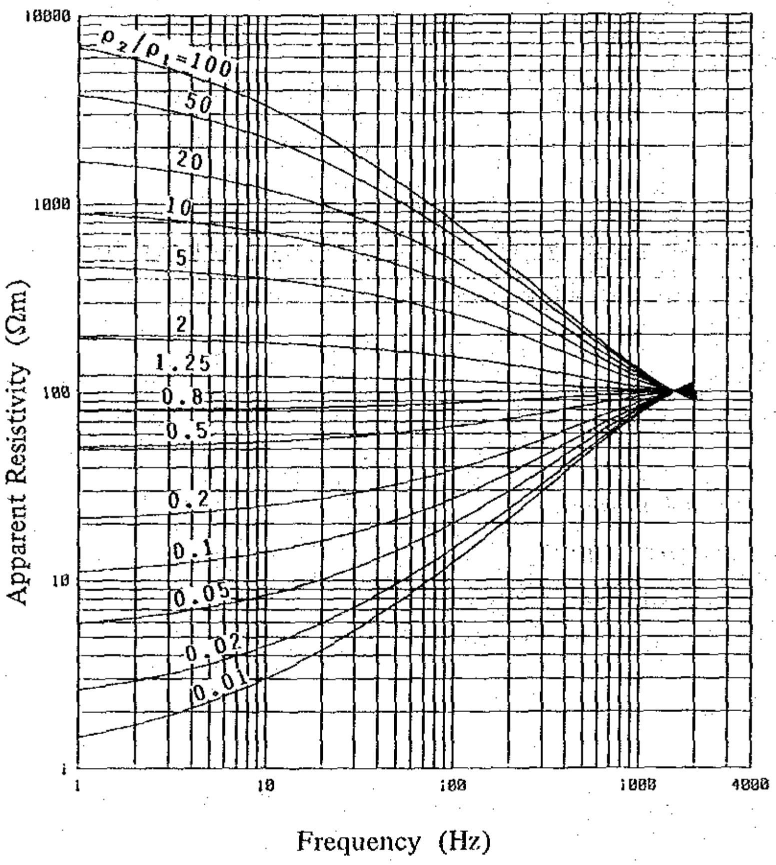

	Resistivity	Thickness
First layer	ρ_1=100Ωm	100 m
Second layer	ρ_2	∞

2-3 Survey Results

As mentioned before, 10 frequencies in the AMT range were used in order to obtain more information related to the geological structure under investigation. The apparent resistivities obtained for every frequency were initially analyzed by drawing apparent resistivity plan maps and pseudosections.

Among the information obtained from the 10 frequencies, those at the frequencies of 2,048, 1,024, 512, 256 and 64 Hz were more carefully analyzed in accordance with the purpose of the survey. They are illustrated in the Figs. III-6 through III-10. Fig. III-11 shows the apparent resistivity pseudosections of six lines taken perpendicular to the main geological structure extending to the NE-SW direction.

Using the results of the one-dimensional analysis made for every station, interpreted resistivity structures were determined for six sections and indicated in the Fig. III-12 through III-14. Interpreted resistivity maps were also drawn at the depths of 100m, 300m and 500m and are shown in the Fig. III-15 through III-17.

2-3-1 Apparent Resistivity Plan Maps

The apparent resistivity shows a strong resistivity contrast and permits us to divide the resistivity distribution into three areas, namely, the western part indicating a high resistivity, the central part with a middle resistivity, and the eastern side which shows a low apparent resistivity. The analysis of these three distributions indicates many resistivity discontinuities of extensions N-S, NE-SW, reflecting a complicated geological structure. The analysis of the maps at the different frequencies seems to indicate a nearly similar feature.

The following are the detailed distribution of apparent resistivities shown on five plan maps:

2048 Hz

This plan map which was drawn using the highest frequency, indicates shallower information. Resistivities higher than 1,000Ωm are seen to the west, northwest, center and northeast of the survey area.

The high resistivities in the west extend in the N-S direction and at bigger scale compared to other areas.

The northwest area can be seen as formed by two resistivity zones expanding to the north and indicating a three-dimensional distribution.

The central area seems to be caused by a part of the same highly resistive bodies as that of the northwest area which may be divided by a presumed fault structure separating both areas.

The northeast high resistivity area is seen scattered to the N-S direction.

Resistivities of less than 100Ωm are seen around the center of the area and all over the east. This central area is spread in such a way that splits the above-mentioned high resistivity of the northwest, west and central areas. If the resistivity contour line of 150Ωm is included, this area is distributed along the N-S direction. The strong resistivity contrast seen around this low resistivity area, suggests a large geological structure towards the N-S direction.

The low resistivity shown all over the east area forms a large low resistivity zone trending toward the N-S direction. It seems to reflect the effect caused by the conductive layer which is distributed horizontally from the surface to a shallower portion and stretching eastwards to the outside of the survey area.

The middle resistivity form 150 to 600Ωm which is found distributed around the central area toward the NE-SW direction, controls the two areas of low resistivity distributions.

It is specifically in this resistivity zone from 300 to 600Ωm that the C-1 ore deposit is found and where the CPRM has carried out almost all the previous surveys.

1024 Hz

Resistive zones higher than 1,000Ωm are seen to the west and center of the survey area. The former, which is found separating the west and northwest areas of the above-mentioned 2048 Hz map, suggests a wide distribution of highly resistive rocks. The latter is distributed so that the area is continued by several independent small areas. The arrangement of these small areas is quite interesting and seems to be caused by an up-and-down movement (folding) of resistive rocks distributed along the NE-SW direction.

Low resistivities less than 100Ωm are scattered to the east and center of the survey area. Those in the east are distributed along the NNE-SSW direction and constitute a low resistivity zone of large scale and the extent is more or less equal to the high resistivities shown in the west. On the other hand, the center area appears to reflect either the effect of the fault structure along the N-S direction or the fracture zone in the boundary of the stratum.

Distribution of the middle resistivity from 150 to 600Ωm is seen to be extending along the NE-SW direction about 5km between the high resistivity area of the whole west area and the low resistivity area of all over the east. The extent of this distributed area is almost the same as the one mentioned in the 2048 Hz range. According to the geological map, the highly resistive zone in the west area corresponds to Pip_5, however the high resistive in the center coincides with Pip_4vxt_3. The low resistivity distribution over the east corresponds to Pip_4vxt_1. Notwithstanding the above, the resistivity of Pip_5 cannot be considered higher than 1,000Ωm, and is assumed that the resistive area in the west reflects highly resistive rocks underlying Pip_5.

512 Hz

The resistivity distribution in this frequency shows almost the same general feature as the 1024 Hz range. However, it shows an expansion of the resistive zone, reaching the high resistivity of the west and occupying about 1/3 of the whole survey area stretches westward to the outside of the survey area.

Same as the above area, the resistive zones in the center expands as the frequency decreases, and extends conspicuously toward the NNE direction. Naturally, with the increase of these resistive areas, the low and middle resistivity distributions are seen to be decreased. However, the low resistivity area which splits this survey area constitutes a kind of low resistivity zone along the N-S direction and suggests the existence of a big scale stractural line, which is presumed to have the homogeneous resistive rocks to its west side, and a sort of complicated geological structure to its east side. On the other hand, the low resistivities in the east are seen decreased more in its extension and partly showing the resistivity distribution from 150 to 300Ωm.

256 Hz

As mentioned above, the high resistivity distribution seems to increase its extent.

The high resistivity of the west appears to be connected to the center, showing an H-shape pattern. The high resistivities of the northeast area trending towards the NE-SW direction appear to show no change.

On the other hand, the low resistivities in the east decreases markedly its extend, which are seen only at the southeastern edge of the survey area, and the resistivity increases to 150 through 160Ωm. The conductive layer can be considered as the thin layer distibuted in the shallower part from the surface, and underlying on this, a resistive zone is found to be distributed.

64 Hz

As an interesting fact, the low resistivity area which was seen all over the east in the high frequencies, had changed to a high resistivity distribution with resistivities higher than 1,000Ωm and extending toward the NE direction.

The high resistivity area located in the west of the survey area, shows as a matter of fact the same pattern indicated all the above-mentioned frequency ranges. However, the high resistivity in the center has experience large change in its distribution and is connected to the east.

The low resistivity of less than 100Ωm is notably distributed along the N-S direction crossing the center of the survey area. The low resistivity distribution to the south found at this frequency, suggests the existence of deeper conductive layers.

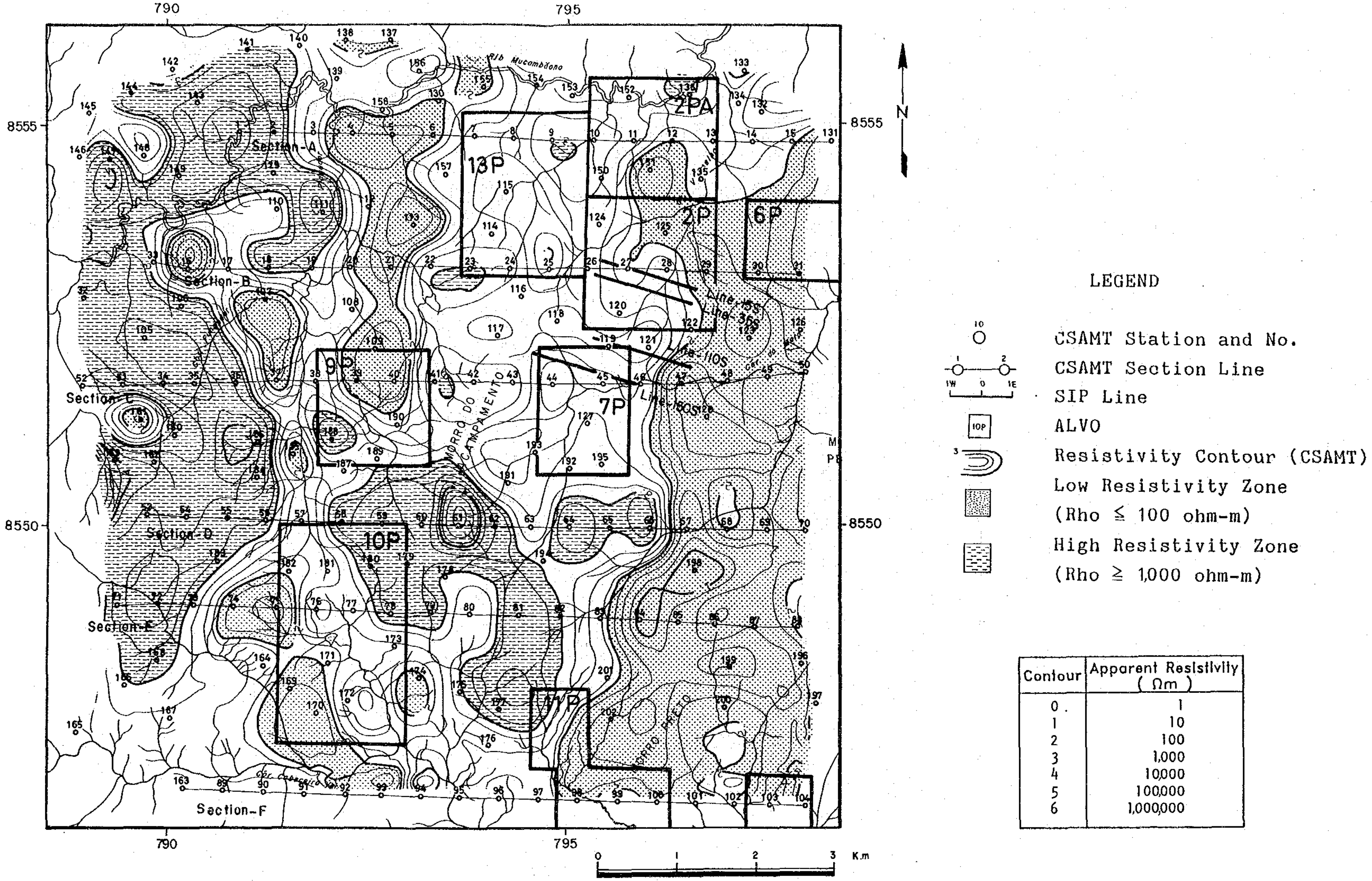

Contour	Apparent Resistivity (Ωm)
0	1
1	10
2	100
3	1,000
4	10,000
5	100,000
6	1,000,000

Fig. III–6 Apparent Resistivity Map [CSAMT (2048 Hz)]

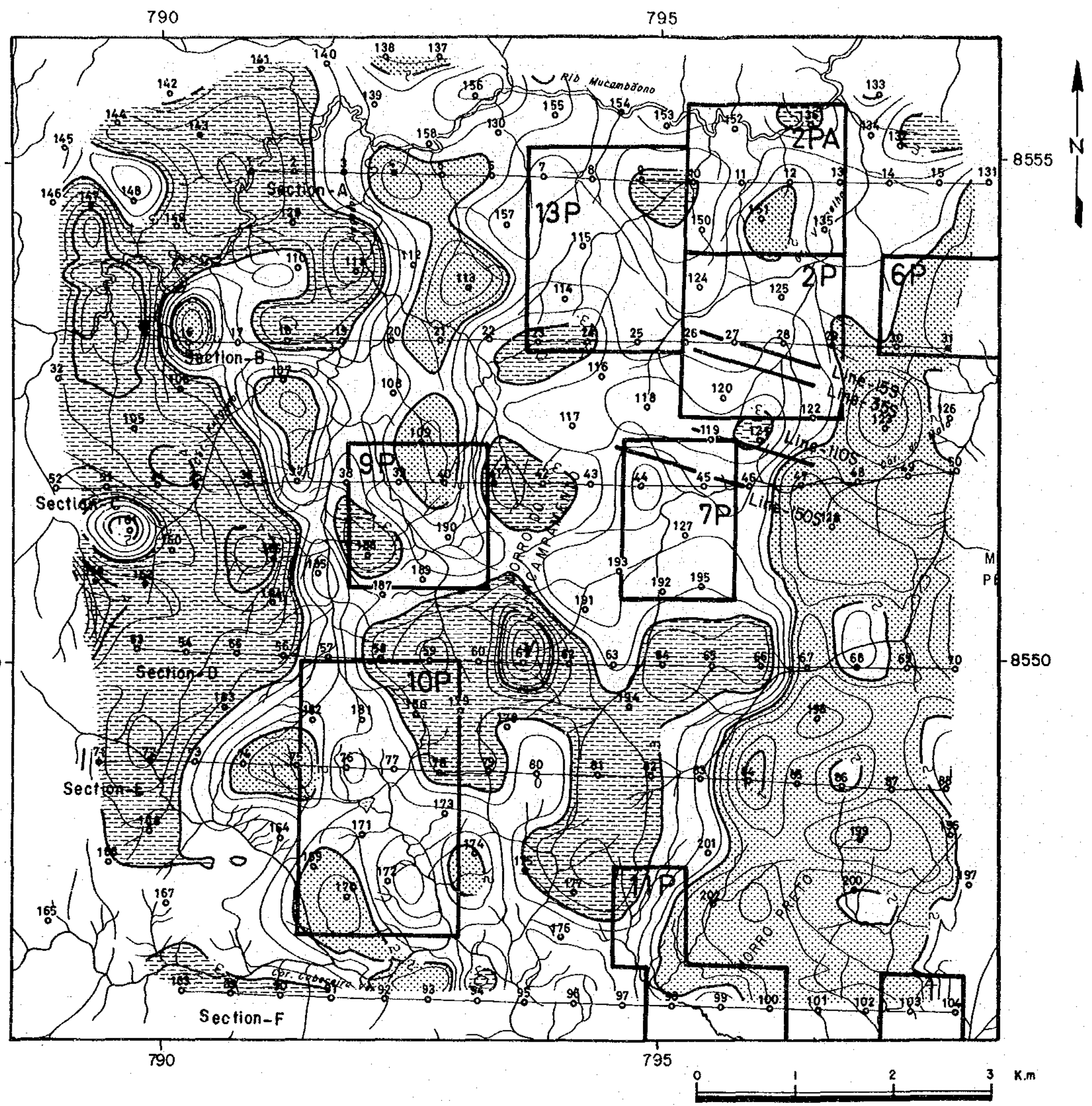

LEGEND

- CSAMT Station and No.
- CSAMT Section Line
- SIP Line
- ALVO
- Resistivity Contour (CSAMT)
- Low Resistivity Zone (Rho ≦ 100 ohm-m)
- High Resistivity Zone (Rho ≧ 1,000 ohm-m)

Contour	Apparent Resistivity (Ωm)
0	1
1	10
2	100
3	1,000
4	10,000
5	100,000
6	1,000,000

Fig. III–7 Apparent Resistivity Map [CSAMT (1024 Hz)]

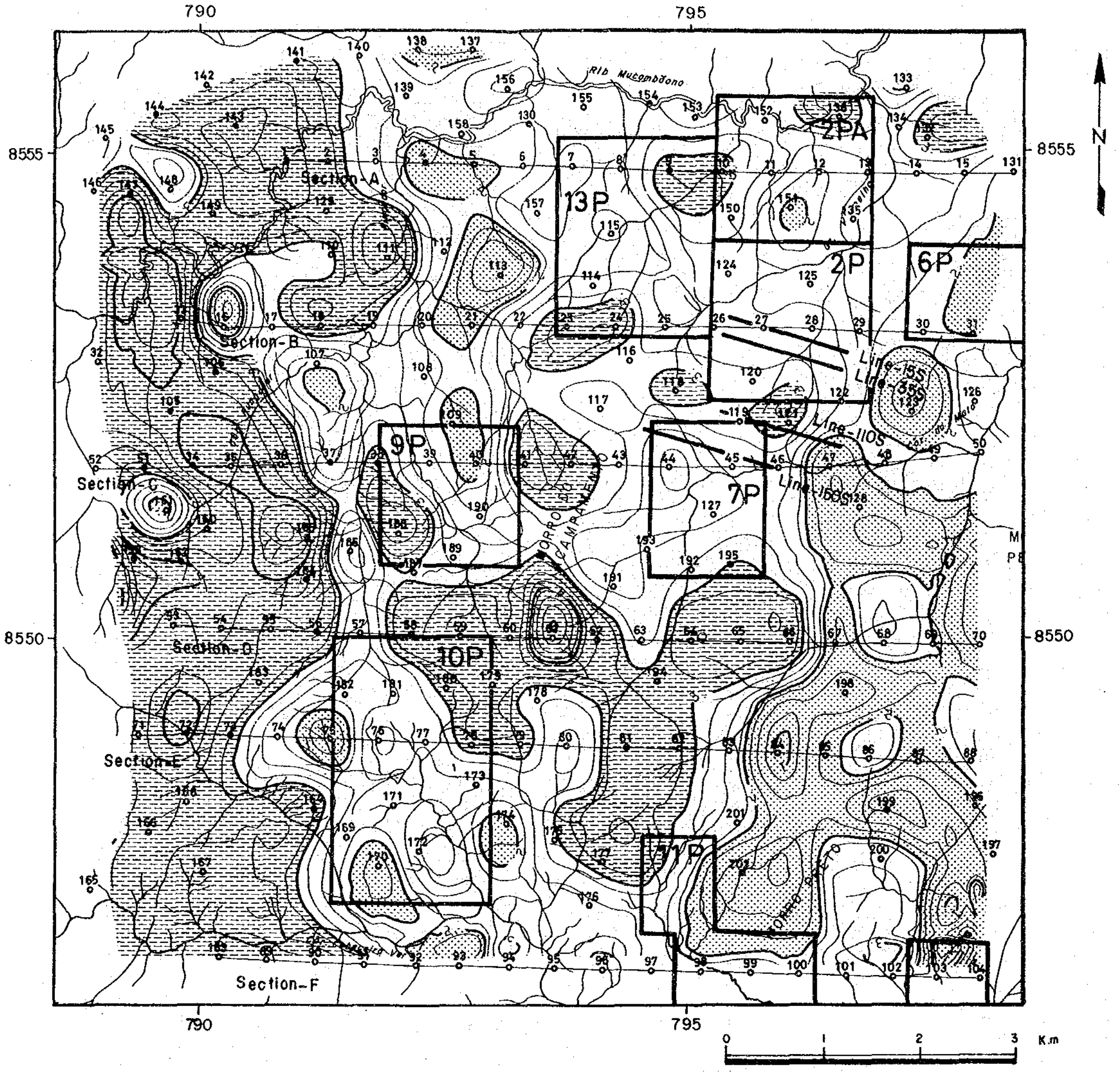

LEGEND

- CSAMT Station and No.
- CSAMT Section Line
- SIP Line
- ALVO
- Resistivity Contour (CSAMT)
- Low Resistivity Zone (Rho ≦ 100 ohm-m)
- High Resistivity Zone (Rho ≧ 1,000 ohm-m)

Contour	Apparent Resistivity (Ωm)
0	1
1	10
2	100
3	1,000
4	10,000
5	100,000
6	1,000,000

Fig. III–8 Apparent Resistivity Map [CSAMT (512 Hz)]

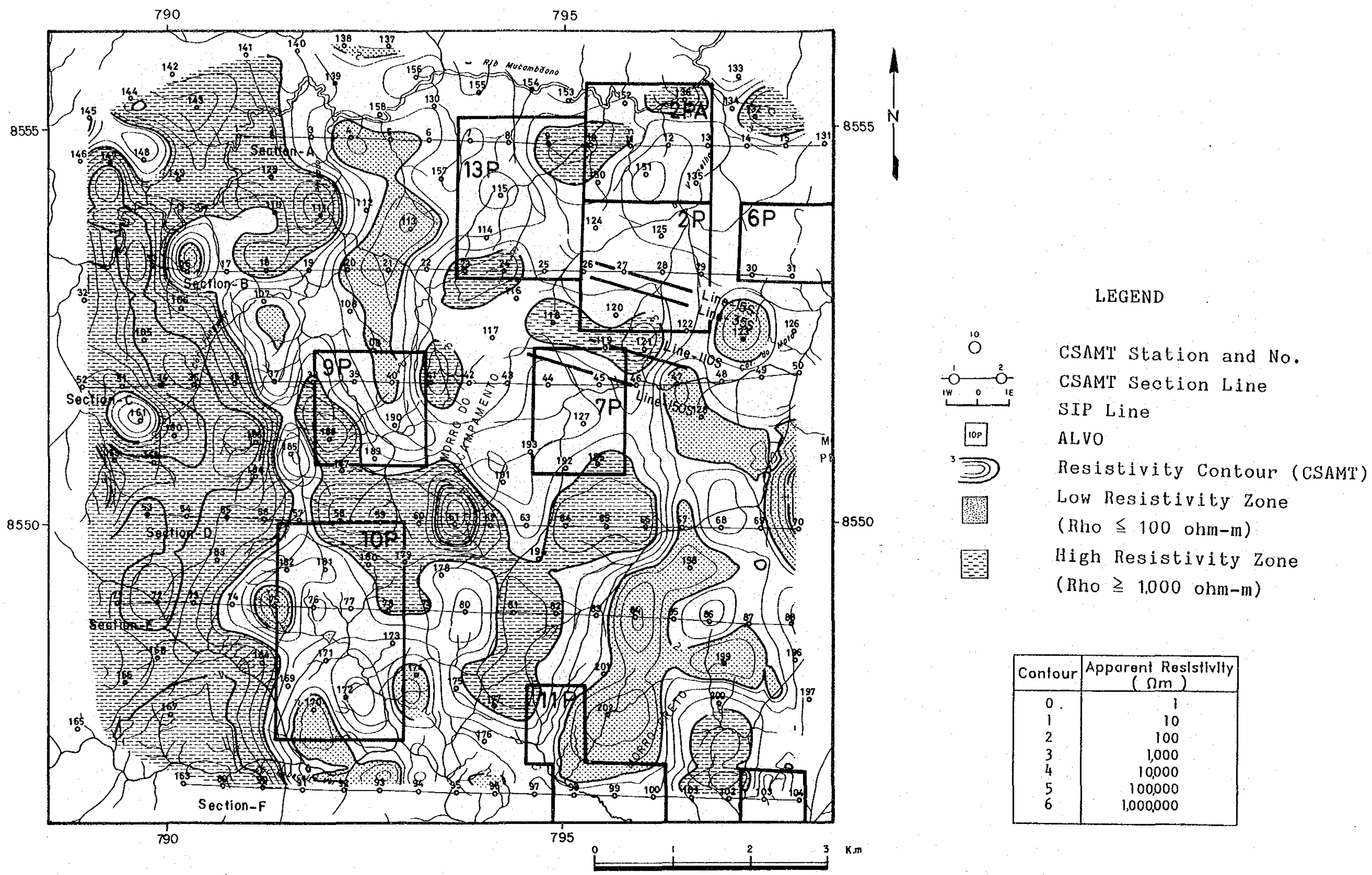

Contour	Apparent Resistivity (Ωm)
0	1
1	10
2	100
3	1,000
4	10,000
5	100,000
6	1,000,000

Fig. III–9 Apparent Resistivity Map [CSAMT (256 Hz)]

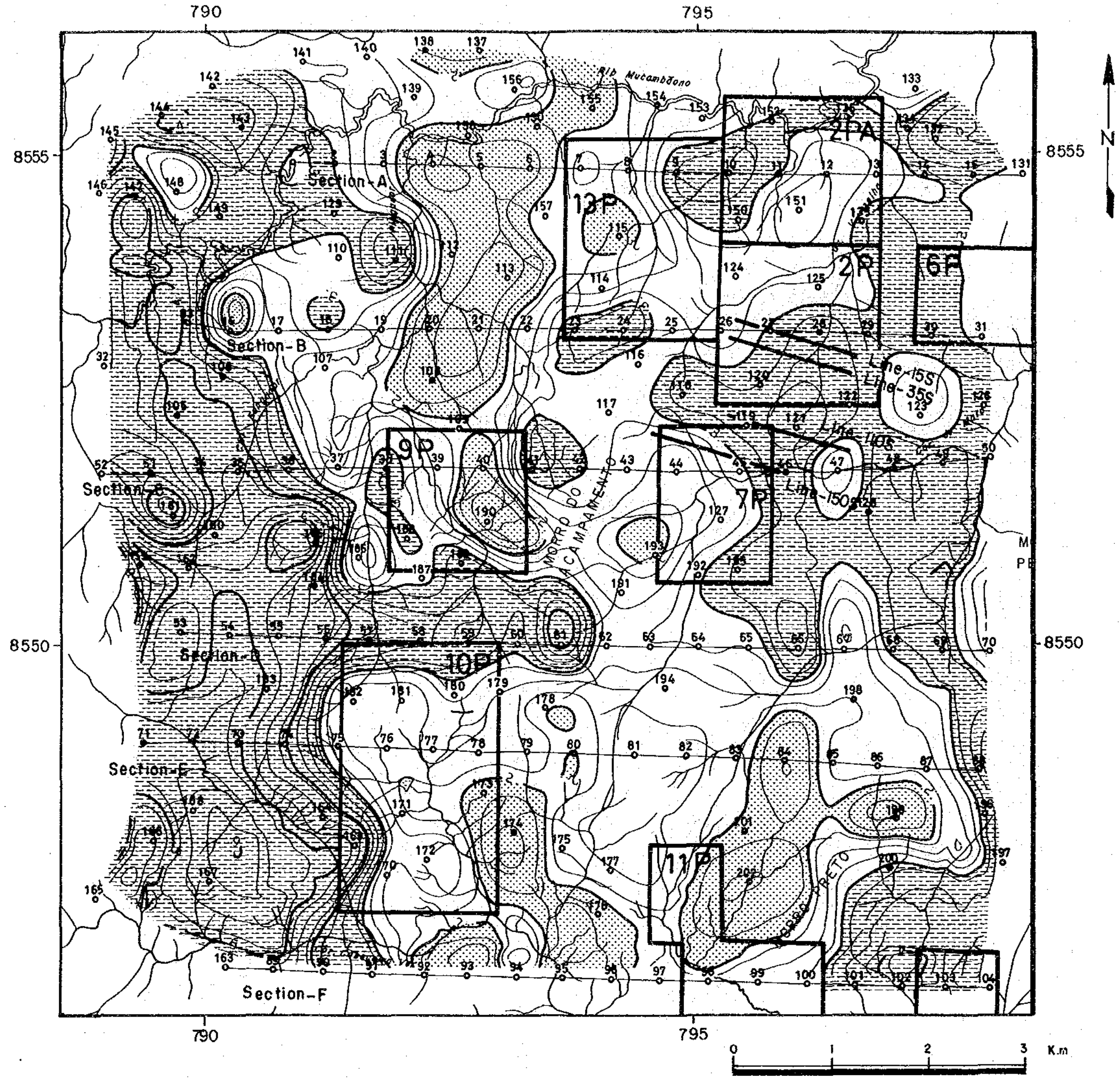

LEGEND

- CSAMT Station and No.
- CSAMT Section Line
- SIP Line
- ALVO
- Resistivity Contour (CSAMT)
- Low Resistivity Zone (Rho ≦ 100 ohm-m)
- High Resistivity Zone (Rho ≧ 1,000 ohm-m)

Contour	Apparent Resistivity (Ωm)
0	1
1	10
2	100
3	1,000
4	10,000
5	100,000
6	1,000,000

Fig. III−10 Apparent Resistivity Map [CSAMT (64 Hz)]

2–3–2 Apparent Resistivity Pseudosections

In order to fulfill the purpose of this survey, five lines, A, B, C, D and E, were placed along the E-W direction, in addition to line F running from north to south as shown in the Fig. III–4.

Using the data obtained from the stations located on those lines, apparent resistivity pseudosections were plotted as shown in Fig. III–11, with plotting frequency in the vertical direction and receiver position along the horizontal axis.

The analysis of the apparent resistivity distributions show a strong resistivity contrast and some resistivity discontinuities which suggest boundary layer or fault structures.

SECTION–A

In this section, resistivities higher than 1,000Ωm are found not only to the west of Station No. 3, but also between Station No. 8 and No. 11 and between Station No. 13 and No. 131.

As to the high resistivity to the west of Station No. 3, it was detected from the high to low frequency range, giving indications to extend westward. Between Station No. 8 and No. 11, resistivities from 500 to 1,000Ωm are detected at 2048 Hz reflecting the effect of a conductive layer distributed at shallow depths. Notwithstanding the above, between these stations and at less than 1024 Nz, the resistivities were higher than 1,000Ωm. Between Station No. 13 and No. 131, the high resistivities found at the frequency range of less than 32 Hz are seen to be connected to the above-mentioned locations.

These high resistivities related to the low frequency range are considered to reflect the same highly resistive rocks (layers), which separate the resistivity distributions into blocks by fault structures.

Low resistivity of less than 100Ωm is found at the low frequency range between Station No. 4 and No. 6, and at a high frequency range at Station No. 131.

SECTION–B

This section passes through the C-1 ore deposit, showing a similar resistivity distribution as that of Section–A. However, in this section, both sides of Station No. 21 show different resistivity distributions, reflecting different structures. In the west of Station No. 21, some resistivity discontinuities are shown distinguishing in the block structures of high and low resistivity. On the other hand, in the east of this station is indicated a distribution which suggests a horizontal structure.

The high resistivity of more than 1,000Ωm found between Station No. 23 and No. 24 at the frequency range of less than 1,024 Hz, suggests that high resistivity is distributed at shallow depths.

Comparing the low resistivity of less than 100Ωm found in this section with that of Section–A, the low resistivity between Station No. 20 and No. 21 is distributed less. However, the low resistivity found partly to the east of Station No. 12 at the high frequency range, is seen widely distributed from the east of Station No. 25 in this section.

SECTION–C

In this section, the resistivity higher than 1,000Ωm suggests the existence of a high resistivity layer widely distributed. The high resistivity of more than 1,000Ωm can be seen in the west of Station No. 36 through the whole frequency range. However, to the east of Station No. 45, it is widely distributed at the frequency range of less than 128 Hz.

Low resistivities of less than 100Ωm are found below Station No. 37, between Station No. 39 and No. 40, and to the east of Station No. 47. The latter is distributed horizontally above the high resistivity and considered to reflect the shallow conductive layer. The one between Station No. 39 and No. 40 gives indications of a deeper conductive layer being extended to the south of Section–A.

SECTION–D

The resistivity distribution seen in this section reflect a monotonic geological structure and generally shows although not in the area to the east of Station No. 67, a high resistivity of more than 1,000Ωm, indicating the existence of a wide resistive layer. However, the low resistivity found to the east of Station No. 67 suggests the existence of a layer connected from the east of Station No. 47 of Section–C. Noticeable faults are presumed around Station No. 57, between Station No. 63 and No. 66.

SECTION–E

The high resistivity in connection with the low resistivity distribution as seen in this section, seems to separate several blocks by fault structures in a remarkable way, showing a complicated geological structure. The high resistivity of more than 1,000Ωm seems to be continued from Section–D. However, its distribution form of several blocks separated by discontinuity lines, reflects the existence of the fault structures.

Low resistivities of less than 100Ωm are found between Station No. 74 and No. 75, below Station No. 78 at the frequency range of less than 32 Hz, and to the east of Station No. 83. The one found between Station No. 74 and No. 75, reflects the effect of fault and fracture zone. Fault structures are presumed to the east of Station No. 83, where a low resistivity effect is distributed at shallow depths.

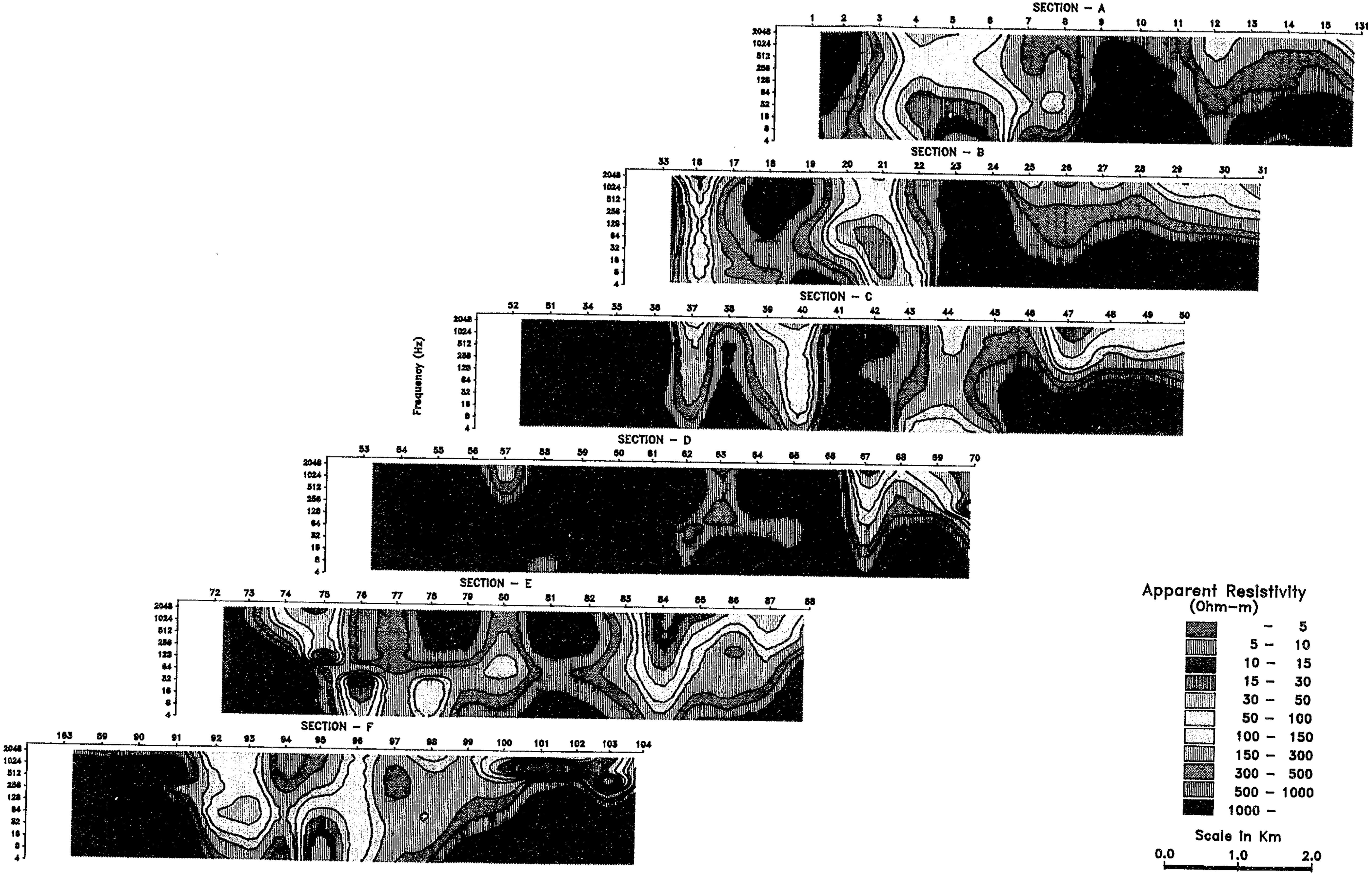

Fig. III-11 Apparent Resistivity Pseudo-sections (Section A–F)

SECTION–F

In this section, distribution of the high resistivities is seen at the both ends of the seciton and a strong resistivity contrast between high and low resistivities is shown.

The high resistivities detected in the area to the west of Station No. 91, and at the frequency range of less than 256 Hz to the east of Station No. 98, are considered the same as those detected at the both ends of Section–E, suggesting this fact, the continuity of high resistivity layer toward the N-S direciton. In the area of the east of Station No. 98 at the frequency of more than 512 Hz, the low resistivity distribution is considered to reflect a thin conductive layer laying on a resistive layer. The low resistivities shown between Station No. 92 and No. 93 are considered to be the southward extension of the low resistivities indicated between Station No. 74 and No. 75 of Section–E and presumed to dip eastward. A conductive layer appears around the surface between Station No. 96 and No. 99, with a resistive layer of 1,000–2,000Ωm being distributed below this layers.

Noticeable fault structures are presumed to exist around Station No. 91, No. 94, No. 99 and between Station No. 102 and 103.

2–3–3 **Resistivity Sections**

Resistivities at depths of less than 2,000m were derived from 1-D model calculation which assumes a multi-layer horizontal structure. The results were plotted as shown in the structural sections of Fig. III–12 through III–14.

SECTION–A

In this section, three-layer structure, including a thin conductive layer, is predominant but some differences in the resistivity structure are found between Station No. 8 and No. 9.

Between Station No. 5 and No. 8, a thick layer of less than 500Ωm including a conductive layer of less than 100Ωm can be seen. The thickness of this layer is over 1,500m between Station No. 5 and No. 6 and about 750m between Station No. 7 and No. 8. This layer may correspond to the third layer at the west of Station No. 3 and the second layer at the east of Station No. 8, which is a thin conductive layer compressed by the rising of the highly resistive layer.

A resistive layer of 1,000 through 10,000Ωm can be seen at the west of Station No. 4, as well as between Station No. 9 and No. 10 and to the east of Station No. 12. They are represented by the first and third layers to the west of Station No. 4, increasing in thickness the first one and decreasing in the third one, both towards the west. Between Station No. 9 and No. 10, this resistive is indicated by the first layer, with a thickness of about 250m dipping westward. This resistive is also indicated by the deepest layer below Station No. 12 and by the second layer to the east of Station No. 13. With regard to the thickness, it is about 500m between Station No. 13 and No. 14, and about 1,000m to the east of Station No. 14. Resistive layer of more than 10,000Ωm is also indicated by the deepest layer at the east of Station No. 7 and between Station No. 9 and No. 11, at a depth of about 250m, dipping eastward.

A comparison of the above layers with geology shows that the resistivity of 1,000 – 10,000Ωm to the west of this section corresponds to Pip_3 of about 100m thickness dipping westward. Between Station No. 7 and No. 8, Pip_4xt_2 of about 500m thickness, is distributed over Pip_3. To the east of a fault structure presumed between Station No. 6 and No. 7, Pip_3 can be corresponded to the third layer between Station No. 7 and No. 8 and the first layer between Station No. 12 and No. 13.

Finally, the highly resistive layer indicated by the deepest layer to the east of Station No. 7 is considered to reflect the basement rocks, which are presumed to be at about 250m depth between Station No. 9 and No.11.

SECTION–B

Through the modeling, conductive layers of less than 100Ωm were found between Station No. 16 and No. 18, between Station No. 20 and No. 22, and to the east of Station No. 25. They have a thickness of about 50m for the first layer between Station No. 16 and No. 18, 50–70m for the first and third layers between Station No. 20 and No. 22, and about 50m for the first layer at the east side of Station No. 25.

The first thin layer of about 50m thickness between Station No. 20 and No. 22 and at the east side of Station No. 25 is considered to reflect Pip_3 which was found distributed in Section–A.

On the other hand, resistive layers of 500 through 1,000Ωm were found for the first and second layers between Station No. 33 and No. 16 and between No. 20 and No. 22 and for the third layer between Station No. 23 and No. 25 and between Station No. 27 and No. 29. These layers are considered to correspond to Pip_4xt_2 which is thickly distributed westward, and to amphibolite which is either weathered or fissured. The third layer existing between Station No. 23 and No. 27 is seen to have a resistivity of 500 through 1,000Ωm which is considered very different from the very high resistivity above and below that layer. It is presumed to be due to the fissured zone which serves as the boundary of the basement rocks and means, therefore, that the second layer can be compared to the compact amphibolite, and the third layer, to the fissured amphibolite. Another resistive layers considered to reflect the compact amphibolite are the second layer between Station No. 17 and No. 18 and distribute near the ground surface in

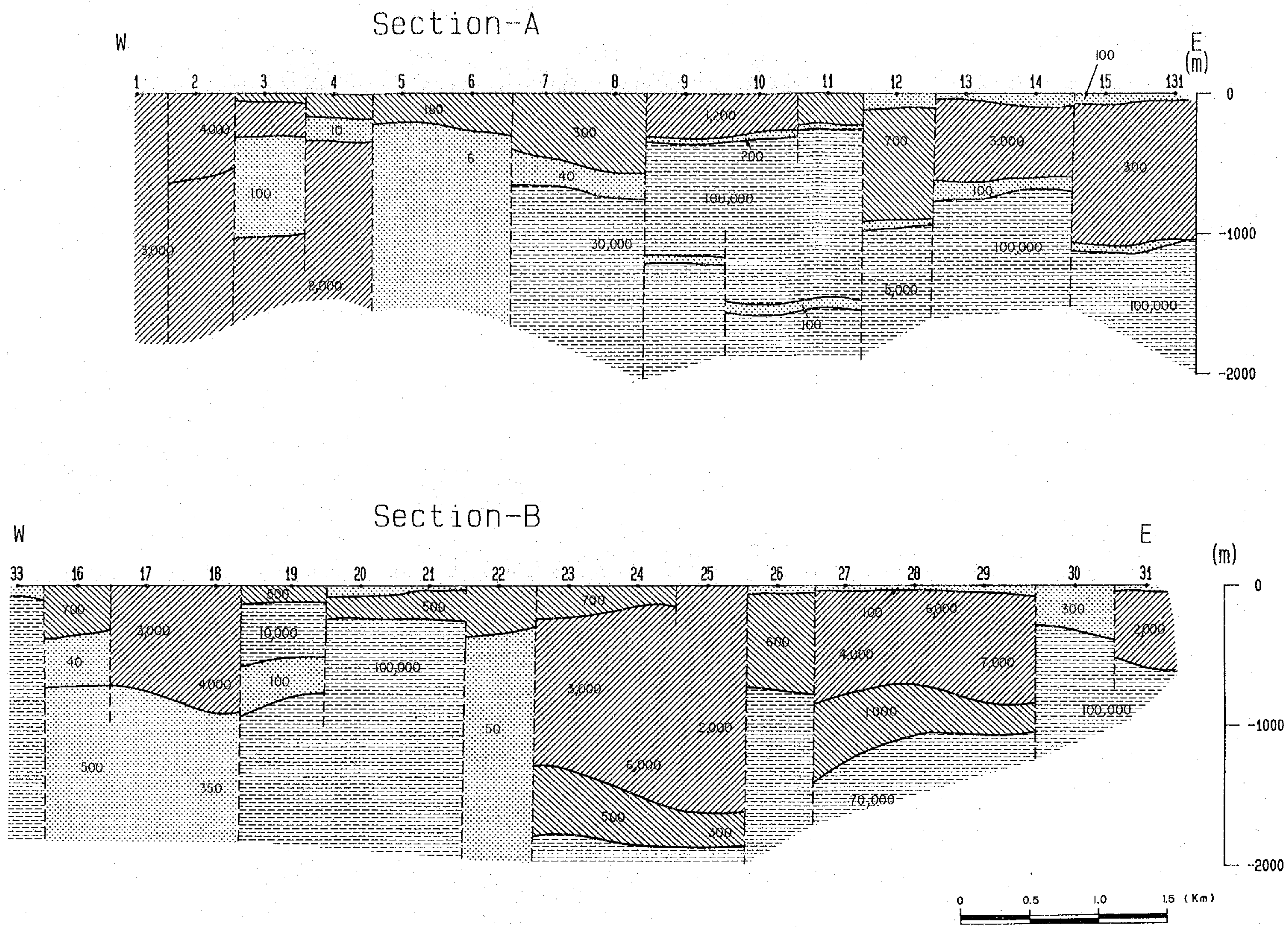

Fig. III-12 Interpreted Resistivity Sections (Sections A and B)

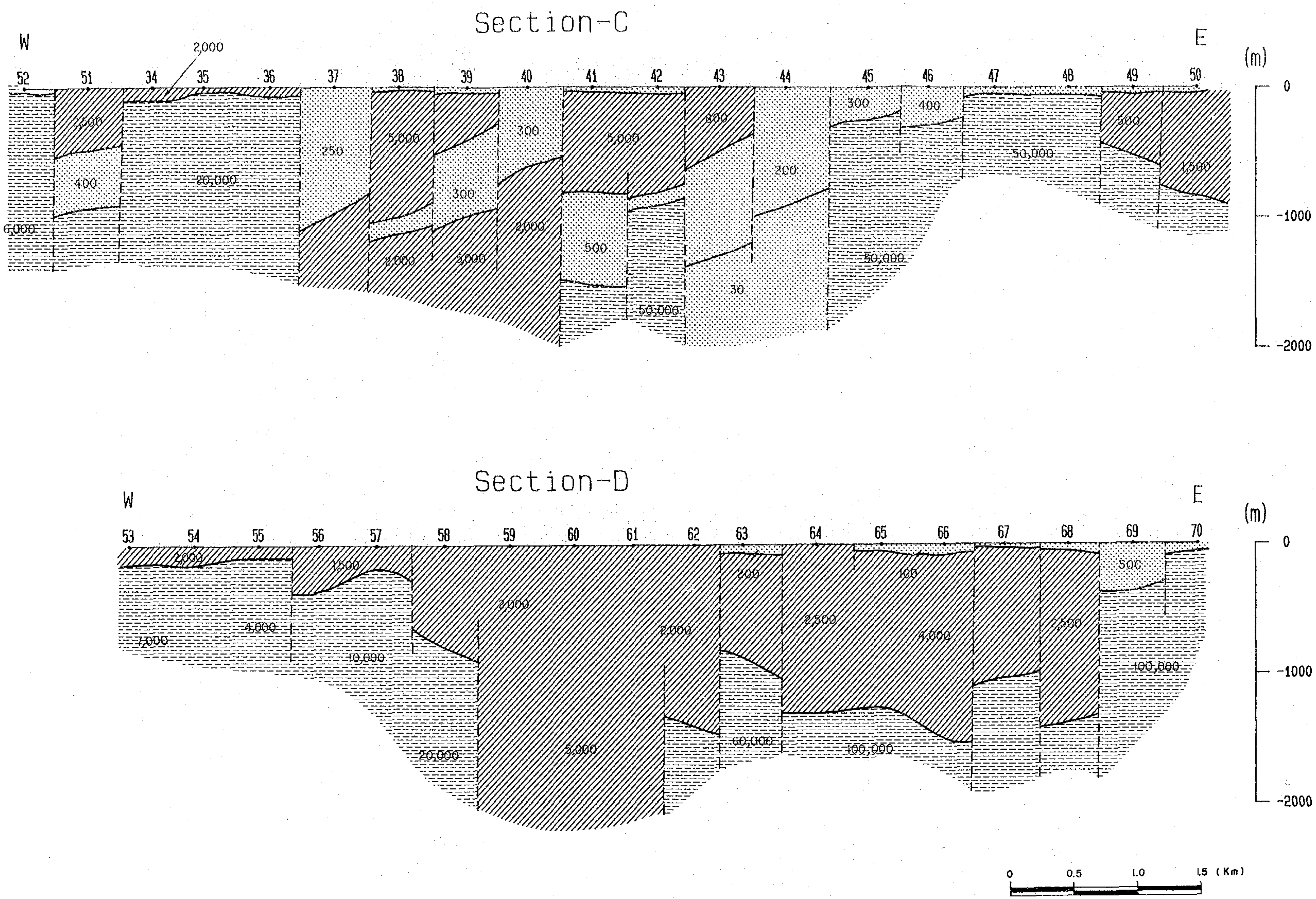

Fig. III-13 Interpreted Resistivity Sections (Sections C and D)

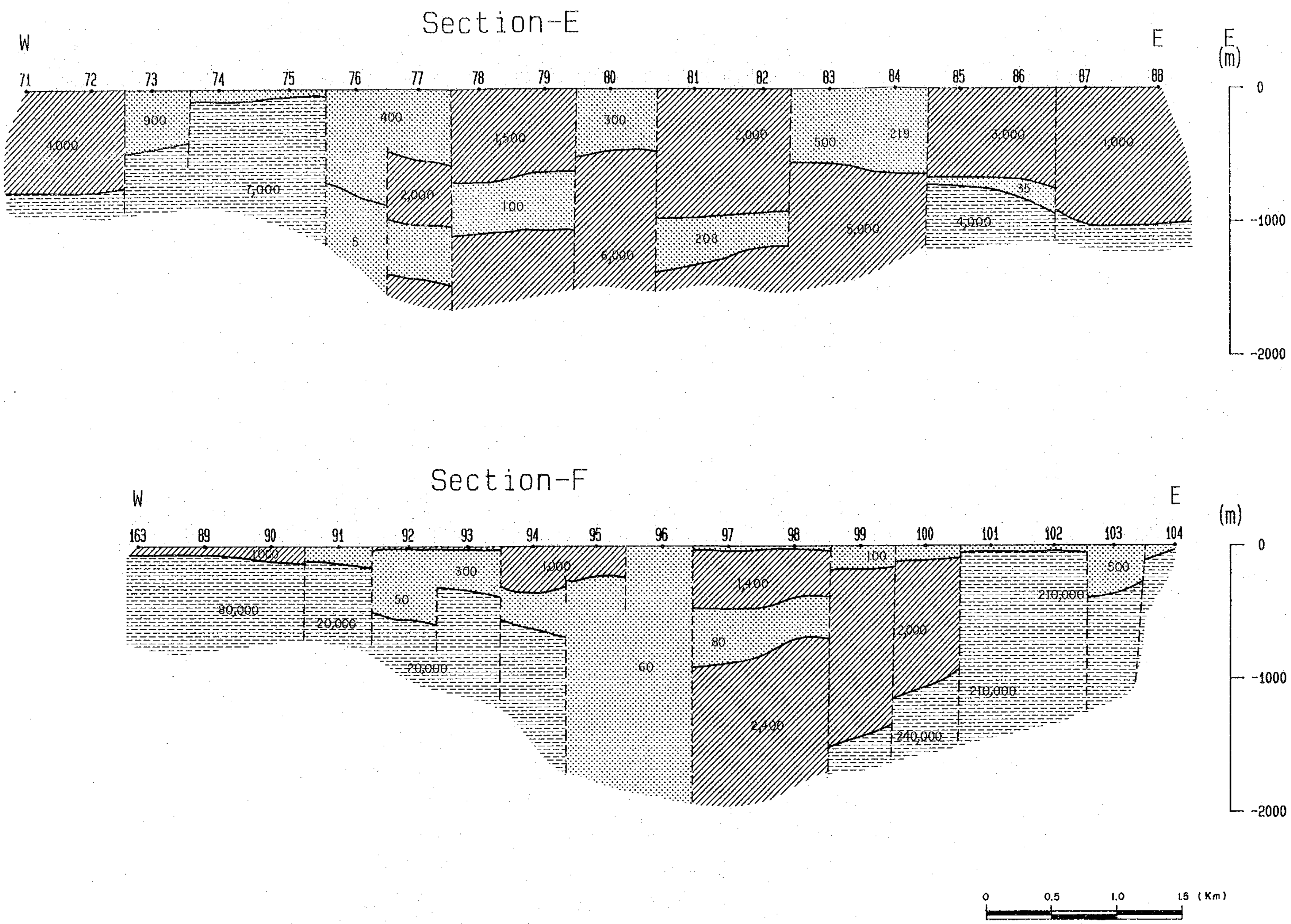

Fig. III–14 Interpreted Resistivity Sections (Sections E and F)

the west of Station No. 31.

The deepest layer of more than 10,000Ωm corresponds to the basement rock, which in this section, is seen deeper than that in Section–A.

Several fault structures are also seen between Station No. 18 and No. 19, between Station No. 20 and No. 21, between Station No. 23 and No. 24, between Station No. 24 and No. 25, between Station No. 26 and No. 27, between Station No. 29 and No. 30 and between Station No. 30 and No. 31.

SECTION–C

A resistivity structure reflecting a complicated geological structure is found between Station No. 37 and No. 45.

Below Station No. 44, a layer of more than 500Ωm, which is a thin layer near the ground surface in Section–B, has a thickness of more than 2,000m, then it is thought that this layer shows a three-dimensional distribution of Pip_3.

A resistive layer of 1,000–5,000Ωm found between Station No. 38 and No. 42 is considered to be a southern extension of a resistive layer reflecting amphibolite between Station No. 21 and No. 25 in Section–B. This layer shows a westward dipping in this section.

A highly resistive layer reflecting the basement rocks is found near the ground surface at both ends of this section, and takes the form of concave distribution around the center of this section.

SECTION–D

This section shows a three-layer structure, that is, the first and second layers with resistivities of 1,000–5,000Ωm, and the deepest layer with resistivity of more than 5,000Ωm reflecting the basement rocks.

Upper two layers increase those thickness eastward and show 1,300m thick between Station No. 64 and No. 66.

The deepest layer is distributed at shallower depth than in Section–C, in particular toward the west of Station No. 59, where shows a depth as shallow as 100m to the east of Station No. 55. This layer tends to distribute widely toward south.

SECTION–E

In this section, a resistivity layer of less than 1,000Ωm can be seen down to about 1,000m in depth, and in further depths is a resistivity layer of more than 5,000Ωm. However, between these two layers, a thin layer of about 100Ωm is found, which is caused probably by a fracture